Chloride (HCl/Cl⁻) dominates inorganic aerosol formation from ammonia in the Indo-Gangetic Plain during winter: Modeling and comparison with observations

Pooja V. Pawar[1,6], Sachin D. Ghude[1], Gaurav Govardhan[1], Prodip Acharja[1], Rachana Kulkarni[2], Rajesh Kumar[3], Baerbel Sinha[4], Vinayak Sinha[4], Chinmay Jena[5], Preeti Gunwani[1], Tapan Kumar Adhya[6], Eiko Nemitz[7], and Mark A. Sutton[7]

[1]Indian Institute of Tropical Meteorology (IITM), Ministry of Earth Sciences, Pune, India
[2]Savitribai Phule Pune University, Pune, India
[3]National Center for Atmospheric Research (NCAR), Boulder, CO, USA
[4]Department of Earth and Environmental Sciences, Indian Institute of Science Education and Research Mohali, Punjab, India
[5]India Meteorological Department (IMD), Ministry of Earth Sciences, Lodhi Road, New Delhi, India
[6]Kalinga Institute of Industrial Technology (KIIT), Bhubaneshwar, India
[7]UK Centre for Ecology & Hydrology (UKCEH), Edinburgh, UK

Correspondence to: Sachin D. Ghude (sachinghude@tropmet.res.in)

Abstract. The Winter Fog Experiment (WiFEX) was an intensive field campaign conducted at Indira Gandhi International Airport (IGIA) Delhi, India, in the Indo-Gangetic Plain (IGP) during the winter of 2017-2018. Here, we report the first comparison in South Asia of high temporal resolution simulation of ammonia (NH_3) along with ammonium (NH_4^+) and total NH_x (= $NH_3 + NH_4^+$) using the Weather Research and Forecasting model coupled with chemistry (WRF-Chem) and measurements made using the Monitor for AeRosols and Gases in Ambient Air (MARGA) at the WiFEX research site. In the present study, we incorporated Model for Simulating Aerosol Interactions and Chemistry (MOSAIC) aerosol scheme into the WRF-Chem. Despite simulated total NH_x values/variability often agreed well with the observations, the model frequently simulated higher NH_3 and lower NH_4^+ concentrations than the observations. Under the winter conditions of high relative humidity (RH) in Delhi, hydrogen chloride (HCl) was found to promote the increase in the particle fraction of NH_4^+ (which accounted for 49.5 % of the resolved aerosol in equivalent units) with chloride (Cl^-) (29.7 %) as the primary anion. By contrast, the absence of chloride (HCl/Cl^-) and their chemistry in the standard WRF-Chem model results in the prediction of sulfate (SO_4^{2-}) as the dominant inorganic aerosol anion. To understand the mismatch associated with the fraction of NH_x in the particulate phase (NH_4^+/NH_x), we added HCl/Cl^- to the model and evaluated the influence of its chemistry by conducting three sensitivity experiments using the model: No HCl, Base Case HCl (using a published waste burning inventory), and 3×Base HCl run. We found that 3×Base HCl increased the simulated average NH_4^+ by 13.1 µg m⁻³ and NH_x by 9.8 µg m⁻³ concentration while reducing the average NH_3 by 3.2 µg m⁻³, which is more in accord with the measurements. Thus HCl/Cl^- chemistry in the model increases total NH_x concentration, which was further demonstrated by reducing NH_3 emissions by a factor of 3 (-3×NH_3_EMI) in the 3×Base HCl simulation. Reducing NH_3 emissions in the 3×Base HCl simulation successfully addressed the discrepancy between measured and modeled total NH_x. We conclude that modeling the fate of NH_3 in Delhi requires a correct chemistry mechanism accounting for chloride dynamics with accurate inventories of both NH_3 and HCl emissions.

1 Introduction

The Indo-Gangetic Plain (IGP) is one of the global hotspots of atmospheric ammonia (NH_3) and faces a range of environmental challenges, particularly during the winter season, including adverse air pollution episodes, especially as NH_3 plays a substantial role in secondary aerosol formation (Ghude et al., 2020, 2008b, 2008a; Kumar et al., 2021; Saraswati et al., 2019; Sharma et al., 2020; Singh et al., 2021). Atmospheric NH_3, along with oxides of nitrogen (NO_x), together account for the largest source of reactive nitrogen (N_r), which is primarily emitted by agricultural activities, livestock population, industrial activities, and transportation (Ghude et al., 2009, 2010, 2012, 2013; Móring et al., 2021; Pawar et al., 2021; Sutton et al., 2017b). Ammonia in the environment plays a crucial role in atmospheric chemistry and the eutrophication and acidification of ecosystems (Datta et al., 2012; Mandal et al., 2013; Pawar et al., 2021; Sharma et al., 2008, 2012, 2014b). Control of NH_3 becomes a key priority in an emerging international strategy to manage the global nitrogen cycle (Gu et al., 2021; Sutton et al., 2020). Ammonia is one of the important aerosol precursor gases, and ammonium (NH_4^+) is a major counter ion for the three anions such as chloride (Cl^-), nitrate (NO_3^-), and sulfate (SO_4^{2-}) contributing to $PM_{2.5}$ composition (Seinfeld et al., 2016). In addition, as the dominant alkaline gas in the atmosphere, NH_3 has attracted the interest of scientific researchers since it has been known to promote new aerosol formation both in the initial homogeneous nucleation and in the subsequent growth, especially during wintertime (Acharja et al., 2020, 2021; Ali et al., 2019; Duan et al., 2021; Wagh et al., 2021).

In this study, we focus on wintertime analyses since this season is characterized by low-to-dense fog events, lower temperature (T), and variability of relative humidity (RH), which fluctuates from 40 to 100 % (Ghude et al., 2017; Kumar et al., 2020). Ammonia acts as a neutralization agent for determining the acidity of aerosol particles (Acharja et al., 2020; Ali et al., 2019; Ghude et al., 2017). It also affects $PM_{2.5}$, the acidity of clouds, and the wet deposition of nitrogen by neutralizing acidic species (Gu et al., 2021; Xu et al., 2020). Increasing NH_3 concentration over Delhi compared with the surrounding area leads to an increase in $PM_{2.5}$ concentrations (Sharma et al., 2008, 2012, 2014a), which in turn affects air quality, human health, and climate (Behera et al., 2013; Ghude, 2016; Ghude et al., 2008b; Nivdange et al., 2022; Sutton et al., 2017a; Sutton and Howard, 2018).

Satellite observations (Van Damme et al., 2018; Warner et al., 2017), chemical transport models (CTMs) (Clarisse et al., 2009, 2010; Wang et al., 2020b), and ground-based observations (Pawar et al., 2021) revealed that the IGP is the largest regional hotspot of NH_3 concentrations on Earth. Previous studies have identified various sources of NH_3, for example, agricultural activities, industrial sectors, motor vehicles, garbage, sewage, and urine from rural populations at the global scale (Behera et al., 2013; Huang et al., 2012; Sutton et al., 2008). However, in Delhi, agricultural activity (including surrounding arable and sub-urban livestock farming) is estimated to be the dominant source of NH_3, along with traffic emissions (Kuttippurath et al., 2020; Móring et al., 2021; Sharma et al., 2020), but its emissions are subject to large uncertainty. Globally, various modeling efforts have investigated the relative effectiveness of reducing NH_3 emissions in curtailing $PM_{2.5}$ formation (Gu et al., 2021; Pinder et al., 2007, 2008; Zhang et al., 2020). However, over India, the impact on reducing $PM_{2.5}$ might be limited because NH_3 emission reductions may be more challenging due to its alkaline nature and area-wide sources. Ianniello et al. (2010) and Lan et al. (2021) have investigated the variation of atmospheric NH_3 at an urban and suburban site of Beijing with respect to meteorological factors, where RH was found to be a strong factor in influencing the NH_3 mixing ratio. A few studies over Asia have highlighted the gas-to-particle conversion of NH_3 in Delhi

79   (Acharja et al., 2021; Saraswati et al., 2019) and China and its subsequent impact on the aerosol formation (Wang

80   et al., 2015; Xu et al., 2020). Furthermore, excess NH_3 during fog can also enhance secondary aerosol formation

81   in Delhi during winter (Acharja et al., 2021). However, the wintertime behavior of NH_3 in Delhi in CTMs has not

82   yet been investigated and remains poorly understood (Ellis et al., 2011; Metzger et al., 2006). In a recent study,

83   Pawar et al. (2021) highlighted uncertainties associated with gas-to-particle partitioning of NH_3 in a global model

84   MOZART-4 and found a significant overestimation of NH_3 in the model compared with the measurements. The

85   overestimation of NH_3 in the model led the authors to hypothesize that a source specific NH_3 emission inventory

86   in India, considering agricultural statistics on fertilizer use and animal distribution, was missing. Also, there was

87   a need for a high-resolution regional model with advanced chemistry to resolve the NH_3 emissions on the local

88   scale.

89   The present study utilizes the regional Weather Research and Forecasting model coupled with chemistry

90   (WRF-Chem) interpreted using measurements from the Winter fog Experiment (WiFEX), including NH_3, water-

91   soluble ions in $PM_{2.5}$, other trace gases, and meteorological parameters during December-January, 2017-18. For

92   the first time in South Asia, we discuss and compare the modeled and observed temporal variation in gaseous

93   NH_3, particulate NH_4^+, and total NH_x (= $NH_3 + NH_4^+$). Since we found that the total modeled NH_x matches well

94   with the observations, we investigate the ability of the model to accurately describe the gas-to-particle partitioning

95   of the measurements (MARGA) by evaluating the fraction of NH_x in the particulate phase (NH_4^+/NH_x). We

96   conducted several sensitivity experiments with and without adding anthropogenic waste burning emissions of

97   hydrochloric acid (HCl) in the model. The updated model with HCl/Cl^- chemistry was used to analyze and

98   compare the temporal variation of NH_3, NH_4^+, and total NH_x from the WiFEX measurements.

99   **2. Data and methodology**

100   **2.1 Observational datasets**

101   **2.1.1 Description of MARGA**

102   In the present study, we used the same dataset which was previously published by Acharja et al. (2020)

103   and 2021), which described the aerosol time-series and chemistry measured with a Monitor for AeRosols and

104   Gases in Ambient Air-model 2S instrument (MARGA). The MARGA system has two channels, one for sampling

105   PM_1 and the other for sampling $PM_{2.5}$ for ground-based observations. The MARGA (two sampling boxes,

106   analytical box, and connected pumps) was located inside the Indira Gandhi International Airport (IGIA), New

107   Delhi (28.56° N, 77.09° E), with the inlet PM_1 and $PM_{2.5}$ impactors fixed on the terrace with 2 m long inlet lines

108   sampling outdoor air at 8 m above ground and 2 m above the rooftop. Measurements covered a winter period (19

109   December 2017 to 21 January 2018) with frequent moderate to dense fog events. Following intake through the

110   PM_1 and $PM_{2.5}$ impactors, the air was passed through two parallel inlet tubes 2 m long and 14 mm inner diameter

111   PolyTetraFluoroEthylene (PTFE) to the PM_1 and $PM_{2.5}$ sampling channels of the MARGA. The air flow rate in

112   each MARGA sampling box is regulated to a volumetric flow of 1 m^3 h^{-1}. The measurements are close to real-

113   time, as two sets of syringes are employed to collect the samples in which a set of syringes collects the sample

114   and another set sends the collected samples from the previous hour for analysis. Each MARGA sampling system

115   consists of a steam jet aerosol collector (SJAC) and a wet rotating denuder (WRD) for collecting and measuring

116   water-soluble inorganic particulate species and gases in the ambient air. The continuous coating of the WRD by

117   a thin film of absorption solution (10 ppm hydrogen peroxide (H_2O_2)) allows the diffusion of gases into the

118   absorption solution. By contrast, the low diffusion velocity of sub-micron particles restricts the ability of water-

119   soluble aerosols to diffuse into the absorption solution. The absorption solution is continually changed to replace

120   that abstracted for ion chromatography (IC) analysis of the dissolved gases. The air stream, depleted of gases by

121   the WRD, subsequently enters the SJAC, where the steam enhances water-soluble aerosols to grow, allowing their

122   mechanical capture in a cyclone. The aqueous solutions deriving from two cyclones (for PM_1 and $PM_{2.5}$,

123   respectively) are then supplied to the IC for chemical analysis (Acharja et al., 2020).

124   Ambient surface concentrations of NH_3 along with other trace gases (HCl, nitrous acid (HONO), nitric

125   acid (HNO_3), and sulfur dioxide (SO_2) and water-soluble inorganic components of PM_1 and $PM_{2.5}$ (Cl^-, nitrate

126   (NO_3^-), SO_4^{2-}, NH_4^+, sodium (Na^+), potassium (K^+), magnesium (Mg^{2+}), and calcium (Ca^{2+}) were then quantified

127   online by anion and cation chromatography in the analytical box at an hourly resolution. We have used only $PM_{2.5}$

128   inorganic water-soluble components and the gaseous measurements (available from both the PM_1 and $PM_{2.5}$

129   MARGA collection systems). Since NH_4^+ with the three major anions: Cl^-, NO_3^- and SO_4^{2-} constituted 97.3 %

130   of the total measured ions in $PM_{2.5}$ (Acharja et al., 2020), we consider these four significant ions in our present

131   study. In contrast, the remaining ionic species (i.e., Na^+, K^+, Mg^{2+}, and Ca^{2+}) contributed only about 3 % of the

132   total measured ions and were neglected as it would not impact our present study significantly (Acharja et al.,

133   2020). Anions are separated in a Metrosep A Supp-10 (75/4.0) column with sodium carbonate (Na_2CO_3) and

134   sodium bi-carbonate ($NaHCO_3$) (7/8 mmol l^{-1}) eluent. Whereas for cations separation, a Metrosep C4 (100/4.0)

135   cation column with 3.2 mmol l^{-1} HNO_3 eluent was used (Acharja et al., 2020). To suppress the eluent background

136   conditivity of anion chromatographs, three ion exchange units were used to ensure that the ion exchange unit is

137   regenerated in each analysis. 1 M Phosphoric acid (H_3PO_4) was used for this purpose. This was performed to

138   improve the signal-to-noise (S/N) of the anion chromatographs. Details of the MARGA instrument can be found

139   in Makkonen et al. (2012), Thomas et al. (2009), Twigg et al. (2015).

140   **2.1.2 Quality assurance/quality control (QA/QC) of MARGA**

141   To ensure the observation's accuracy and check the data's quality, we have taken all the precautionary measures

142   during the study. The eluents, absorption, and regenerant solutions were prepared with minimum manual

143   intervention. The operational parameters like anion, cation conductivity, SJAC heater temperature, column oven

144   temperature, and airflow were regularly monitored to keep them within the safe limit. In addition to these, before

145   injection of each sample into the anion and cation IC columns, the Lithium Bromide (LiBr) internal standard

146   solution containing 320 µg l^{-1} lithium (Li^+) and 3680 µg l^{-1} bromide (Br^-) was mixed with each sample to provide

147   calibration of each analysis. This ensures that each analysis is calibrated, and the concentration of gaseous and

148   ionic samples are measured accurately. The PM_1 and $PM_{2.5}$ impactors were typically cleaned fortnightly to remove

149   any material that may stick on the surface and inlets of the impactors. The lower detection limits (LODs) of the

150   species monitored by MARGA were mentioned in Acharja et al. (2021). It shows that concentrations of species

151   like Cl^-, NO_3^-, SO_4^{2-}, NH_4^+, SO_2, and NH_3 were always higher than LODs during the winter period. But,

152   concentrations of species like Na^+, K^+, Ca^{2+}, Mg^{2+}, HCl, HONO, and HNO_3 were sometimes below LODs, but

153   the fraction of it was less than ~10 % of the total observation period. We have omitted these values and treated

154   them as NA. As the fraction of observational hours is less and these species contribute much less to the PM_1 and

155   PM$_{2.5}$ mass concentrations, we believe below LODs values would not significantly deviate our results. The quality

156   of the data obtained was then checked using the ion-balance method. As an additional quality check, the ratio of

157   the sum of cations to anions (neq m^{-3}) was used as an indicator for the viable data. We have checked the cation-

158   to-anion ratio of each hourly sample expressed in the unit of neq m^{-3}. We accepted only those values near to unity

159   and rejected those not within the 10 % error bar limit. Based on this evaluation method, overall, for the campaign,

160   the ratio was near unity (1.06 for PM$_1$ and 0.96 for PM$_{2.5}$). Excellent charge balance between anions and cations

161   measured by the system also confirms that there are no significant contamination issues associated with the aerosol

162   measurements. Values in slight excess of unity may indicate the presence of formate and acetate in the aerosol,

163   which MARGA does not measure. Further detail on the quality control of MARGA can be found in Acharja et al.

164   (2020).

2.1.3 Other ground-based measurements

166   Hourly NO$_x$ measurements were made by the chemiluminescence method, and hourly ozone (O$_3$) measurements

167   were made by the UV photometric method (CPCB, 2011) at the nearest air quality monitoring station (AQMS) of

168   IGIA operated by the Central Pollution Control Board (CPCB). CPCB follows the United States Environmental

169   Protection Agency (USEPA) approved AC32M NO$_x$ and 42M O$_3$ analyzer manufactured by Environment S. A.

170   India Private Limited. We used one-hour monitored NO$_x$ and O$_3$ values in our study. These air quality monitoring

171   stations' quality control and assurance processes were followed as outlined in CPCB (2014, 2020). For data quality

172   of CPCB, we omitted all those observed values which fell below LOD of the instrument (2 µg m^{-3} for NO$_x$ and 4

173   µg m^{-3} for O$_3$) (Technical specifications for CAAQM station, 2019) and above 500 µg m^{-3} for NO$_x$ and 140 µg m^{-3}

174   for O$_3$ and treated them as NA at a given site. For the NO$_x$ and O$_3$ datasets, only a small fraction of data (2 %)

175   were outside the instrument operating ranges specified. This step aims to remove any short-term local influence

176   that the models cannot capture and retain the regional-scale variability because the nearest sites are located in the

177   urban environment. We removed a single spike represented by a change of more than 100 µg m^{-3} in just 1 hour

178   (h) for all the data in CPCB monitoring stations to filter out random fluctuations in the observations. We removed

179   some very high NO$_x$ and O$_3$ values that appeared in the time series right after measurement gaps. Meteorological

180   parameters, including air temperature (T), relative humidity (RH), wind speed, and wind direction, were measured

181   with the automatic weather station (AWS) platform on a 20 m flux tower (Ghude et al., 2017). For detailed

182   information on the measurement site and its meteorological parameters, refer to (Ali et al., 2019).

2.2 WRF-Chem v 3.9.1 model

184   The Weather Research and Forecasting model coupled with chemistry (WRF-Chem v3.9.1) was employed in this

185   study to simulate atmospheric gases and aerosols over Delhi during the peak winter period, starting from 19

186   December 2017 to 21 January 2018. We recently used a similar model configuration to simulate the air quality

187   over Delhi (Ghude et al., 2020; Kulkarni et al., 2020). This study used the Model for Ozone And Related chemical

188   Tracers (MOZART-4) gas-phase chemical mechanism coupled with the Model for Simulating Aerosol

189   Interactions and Chemistry (MOSAIC) aerosol scheme, that simulates SO$_4^{2-}$, NH$_4^+$, NO$_3^-$, methanesulfonate, Na$^+$,

190   Ca^{2+}, Cl$^-$, carbonate, black carbon (BC), and primary organic mass (OC). Other inert minerals, trace elements, and

191   inorganic species are lumped together as different inorganic masses. MOSAIC allows gas-to-particle formation,

192   which includes NH$_3$, HCl, sulfuric acid (H$_2$SO$_4$), HNO$_3$, and methane sulfonic acid (MSA), and also includes

secondary organic aerosols (SOA). Aerosol size distributions are represented by a sectional aerosol bin approach with four size bins (Georgiou et al., 2018). MOSAIC incorporates the thermodynamic and gas-particle partitioning module described by Zaveri et al. (2008). To reduce the computational cost, we selected a 4-bin MOSAIC mechanism that simulates thermodynamic equilibrium and other aerosol processes such as condensation, coagulation, and nucleation. The same mechanism has been widely used with WRF-Chem for simulations outside India (Bucaram and Bowman, 2021; Sha et al., 2019; Yang et al., 2018), but only a limited number of studies have applied it to the Indian domain to include more detailed chemistry and species (Gupta and Mohan, 2015; Jena et al., 2020; Kumar et al., 2018). The SOA formation in MOSAIC is simulated using the volatility basis set approach (Knote et al., 2015). For consistency with the $PM_{2.5}$ MARGA measurements, we have chosen 3-bins according to simulated aerosols size (0.04–0.156 μm; 0.156–0.625 μm; 0.625–2.5 μm) in accordance with the WRF-Chem aerosol size distribution.

The model domain covers the entire northern region of India, but here model simulations are compared with the observations at IGIA, New Delhi (28.56° N, 77.09° E). The domain was set with a horizontal grid-spacing of 10 km in both the latitudinal and longitudinal directions. The model top vertical grid included 47 vertical levels, with the model top set to 10 hPa. The physical parameterization schemes of model configuration are the same as those described by Ghude et al. (2020) and Jena et al. (2021). EDGAR-HTAP (Emission Database for Global Atmospheric Research for Hemispheric Transport of Air Pollution) for the year 2010 at 0.1° x 0.1° grid resolution was used in this study for anthropogenic emissions of aerosols and trace gases ($PM_{2.5}$, PM_{10}, OC, BC, CO, NO_x, etc.) and are scaled to 2018 as per Jena et al. (2021). Biogenic emissions are calculated online using the Model of Emissions of Gases and Aerosols from Nature version 2.1 (MEGAN2.1) (Guenther et al., 2006), and dust emissions are based on the traditional Goddard Global Ozone Chemistry Aerosol Radiation and Transport (GOCART) dust scheme that works with MOSAIC (Ginoux et al., 2001). Fire INventory from NCAR (FINNv1.5) was used in this study for daily open biomass burning emissions that are vertically distributed within the model using Freitas et al. (2007). The chemical initial and lateral boundary conditions come from the global model simulations from the Model for Ozone and Related Chemical Tracers (MOZART-4), and the meteorological initial and lateral boundary conditions are provided from the fifth generation European Centre for Medium-Range Weather Forecasts (ECMWF) atmospheric reanalysis of the global climate (ERA5) with six-hourly temporal resolution. The simulations were reinitialized every fifth day to limit the growth of meteorological errors in our simulations, but the chemical fields were carried forward from the previous simulation.

3. Results and Discussion

3.1 Comparison of temporal variation in NH_3, NH_4^+, and total NH_x using WRF-Chem and MARGA

3.1.1 Diurnal variation

To investigate how well a state-of-the-art chemical transport model performs in capturing the diurnal behavior of NH_3 and NH_4^+, we compared observed and model-simulated diurnal profiles of NH_3 and NH_4^+. Figure 1 displays the comparison of diurnal variation (00:00 to 23:00 Indian Standard Time (IST)) in meteorological parameters (T and RH) at the IGIA site in Delhi (Fig. 1a) along with NH_3 and NH_4^+ averaged over the study period (Fig. 1b) between observations and model. We adopted diurnal variation in emissions from a recent study by Jena et al.

230 (2021). Note that diurnal variability in the model simulations is primarily controlled by the planetary boundary

231 layer mixing. We first investigated the ability of WRF-Chem to accurately predict the meteorological parameters

232 of RH and T, which are important determinants of the gas-to-aerosol partitioning of (semi-) volatile compounds.

233 As shown in Fig. 1a , simulated T and RH are in reasonable agreement with the observations, with the simulated

234 RH values falling in the range of 50–90 %. Overall, it can be seen that the model shows cold and wet bias compared

235 to the observations but shows warm bias (about 2-3 ℃) and dry bias (about 10-12 %) in the afternoon hours. In

236 spite of the small change in the amplitude of the diurnal cycle of RH, the phase characteristics of the diurnal cycle

237 of both T and RH are reasonably well captured by the model. Figure 1b shows that simulated NH_3 and NH_4^+ are

238 very different compared with the MARGA measurements. The model predicts an average NH_3 and $NH_4^+ \pm 1\sigma$

239 mass loading of 56.7 ± 14.3 and 14.7 ± 4.9 µg m^{-3}, respectively, while MARGA measurements indicate an average

240 NH_3 and $NH_4^+ \pm 1\sigma$ mass loading of 28.2 ± 12.4 and 36.9 ± 15.1 µg m^{-3}, respectively. We find the diurnal variation

241 of gas-phase NH_3 is significantly overestimated by the model (Normalised Mean Bias (NMB) = 1.02). On the

242 contrary, NH_4^+ is underestimated by about 60 % (NMB = -0.60). Simulated NH_3 concentrations peak between

243 07:00-09:00 and 22:00-23:00 h with bimodal variation, whilst MARGA shows a single peak around 12:00-13:00

244 h. On the contrary, a nearly flat diurnal profile of NH_4^+ is predicted by the model, whereas the average MARGA

245 NH_4^+ concentration maxima and minima were observed during night-time (16:00-03:00 h) and daytime (03:00-

246 08:00 and 09:00-16:00 h), respectively.

247   We also looked into the average diurnal profile of NO_x and the NH_3 during dense fog events, and the

248 details can be found in the supplement (Fig. S1 and S2 in the Supplement). It is evident that the observed daytime

249 peak of NH_3 did not coincide with NO_x peaks, suggesting that traffic emissions do not contribute significantly to

250 the observed NH_3 rise. The observed correlation between fog water and enhanced NH_3 pulses is consistent with

251 what would also be expected from the evaporation of dew (Sutton et al., 1998; Wentworth et al., 2014, 2016) (S2

252 in the Supplement) but is not sufficient to identify whether it is the main cause of the daytime increase of NH_3. In

253 the future, measurements of the dew water NH_4^+ and the accumulation of dew water would be ideal for

254 illuminating the contributing processes. The daytime increase in NH_3 concentration could be associated with NH_4^+

255 aerosol volatilization driven by an associated sharp change in T and RH (~ 11:00-12:00 h) (Sutton et al., 2009a,

256 2013) off-ground surfaces. The fastest increase in T is 12:00 h, which is indeed when NH_3 was at maximum

257 concentration indicating gas-to-particle partitioning may impact the diurnal behavior of NH_3 at Delhi during

258 winter (Sutton et al., 2009a, 2009b). However, in the model, because the largest increase in simulated NH_3 also

259 precedes the large changes in simulated meteorological parameters, and because the simulated particulate NH_4^+

260 is flat compared to observations, simulated meteorology is ruled out as a significant contribution to high bias in

261 simulated NH_3. Also, the current model does not include the bidirectional exchange of NH_3 with surfaces such as

262 dew and fog water.

263 **3.1.2 Daily mean variation**

264   To assess the validity of the model, the ratio between observed and simulated values (model/obs) was

265 tested. Figure 2 displays the model/obs ratio of daily mean variations in the NH_3, NH_4^+, and total NH_x

266 concentrations. The model shows large differences in NH_3 and NH_4^+ compared with observations. We find a

267 model/obs higher than 1 (1.5-4.5) in simulated NH_3, indicating the model is biased high (NMB = 1.02), while

268 there is a poor agreement for NH_4^+ (model/obs less than 0.5), indicating model is biased low (NMB = -0.62).

There is good agreement between the modeled total NH_x, which is mostly consistent with the observation (model/obs close to 1) with a small bias (NMB = 0.08). Despite the adequate ability of the model to reproduce the accurate total NH_x, the model is biased low for NH_4^+ and high for NH_3, indicating that the model's representation of the gas-to-particle partitioning is not correct. It is, therefore, necessary to understand missing chemical processes in gas-to-particle partitioning responsible for the overestimation of NH_3 and underestimation of NH_4^+ in the model.

3.2 Gas-to-particle partitioning

We investigated the ability of the model to accurately describe the gas-to-particle partitioning of the measurements (MARGA) by evaluating the fraction of total NH_x in the particulate phase (NH_4^+/NH_x) (Ellis et al., 2011; Wang et al., 2015) for which statistical values are summarized in Table 1. The correlation coefficient (r) indicates an inverse relationship of NH_4^+/NH_x with NH_3 for both MARGA and model (r = -0.57, -0.58, respectively). A strong correlation of the MARGA ratio NH_4^+/NH_x with the dominant anion concentration (Cl^-: r = 0.79) was observed. However, the measurement shows a poor relationship between SO_4^{2-} and NH_4^+/NH_x followed by NO_3^-, which is probably due to very low concentrations that do not change NH_4^+/NH_x significantly even when SO_4^{2-} and NO_3^- are neutralized (see Fig. 6). By contrast, the model shows a strong correlation between NH_4^+/NH_x with SO_4^{2-} concentration (r = 0.77). MARGA indicates high particulate fractions of NH_4^+ and Cl^- while the modeled composition is dominated by NH_4^+ and SO_4^{2-}. This mismatch is due to the complete absence of Cl^- chemistry in the standard model. The measured NH_4^+/NH_x suggests that anthropogenic HCl may be promoting this increase in particle fraction of NH_4^+ and Cl^- via partitioning into the aerosol, deprotonating in the aerosol water, followed by NH_3 partitioning and being protonated by the ionization of the strong electrolyte HCl (Chen et al., 2022; Gunthe et al., 2021).

Figure 3 shows the percentage contribution of gases (NH_3, SO_2, HCl, HNO_3, and HONO) and $PM_{2.5}$ aerosol (NH_4^+, SO_4^{2-}, NO_3^- and Cl^-) during the WiFEX measurements. The pie charts for the gases show that NH_3 (accounting for 53.3 % of the measured total gas concentration) dominates the gas phase, followed by sulfur dioxide (SO_2) (35.61 %), whereas $PM_{2.5}$ aerosol show NH_4^+ (49.5 %) as a major cation and Cl^- (29.7 %) as a significant anion followed by NO_3^- (11.7 %) and SO_4^{2-} (9 %). There is also a very high amount of SO_2 reaching the site from the nearby industrial area, which is not converted to SO_4^{2-} very quickly (Acharja et al., 2021). In a normally NH_3-rich atmosphere, gas-phase oxidation of SO_2 is much slower than the aqueous phase oxidation of O_3, and due to nearby sources, much of the sulfur is present as SO_2 (Li et al., 2007) (Fig. S3 in the Supplement). This appears to be because of the slow rate of gas phase oxidation of SO_2. Although the atmosphere is rich in NH_3, in principle favoring aqueous phase oxidation via O_3, it appears that O_3 concentrations are often insufficient (mean = 36.3, median = 33.8, minimum = 26.5, and maximum = 53.9, ug m^{-3} respectively) at the IGIA site (Fig. S3 in the Supplement). Hence for many periods during the WIFEX campaign, SO_4^2 and NO_3^- are very low, with the result that the NH_4^+/NH_x ratio does not change appreciably when SO_4^{2-} is neutralized (Table 1).

According to thermodynamic equilibrium theory, an aqueous solution maintains charge neutralization initially by balancing NH_3 uptake with the uptake of sulfuric acid (H_2SO_4) before HNO_3 and HCl can partition into the aqueous aerosol; hence all SO_4^{2-} in the condensed phase will be fully neutralized before any HNO_3, or HCl can partition (Behera et al., 2013). Typical Delhi winter conditions of excess NH_3, high RH, and low T favor gas-to-particle partitioning of NH_3. The principal inorganic chemical reactions that occur in aqueous atmospheric

308 aerosols form pairs of non-volatile NH_4^+ and acid anions (SO_4^{2-}, NO_3^-, and Cl^-) are summarized in reactions R1

309 to R3 (Seinfeld et al., 1998).

310 $$2NH_{3(g)} + H_2SO_{4(g)} \rightleftarrows NH_4^+ + SO_4^{2-} \tag{R1}$$

311 $$NH_{3(g)} + HNO_{3(g)} \rightleftarrows NH_4^+ + NO_3^- \tag{R2}$$

312 $$NH_{3(g)} + HCl_{(g)} \rightleftarrows NH_4^+ + Cl^- \tag{R3}$$

313

314 NH_4^+ and Cl^- (R3), which are favored by low T and high RH, form a reversible equilibrium with NH_3 and HCl

315 (Ianniello et al., 2011; Seinfeld and Pandis, 2016), which was the case during WiFEX. It is likely that high Cl^- in

316 Delhi resulted from gas–to-particle partitioning of HCl into aerosol water in the presence of excess NH_3 (R3),

317 with aqueous phase Cl^- stimulating further water uptake and jointly driving aerosol mass composition and growth

318 through co-condensation (Chen et al., 2022; Gunthe et al., 2021). Hence, to understand the driver of the measured

319 NH_4^+ and the role of aqueous chemistry, we plotted the fraction of the ratio of HCl to Cl^- (HCl/Cl^-) as a function

320 of NH_4^+ concentration and RH in Fig. 4. Fraction of particulate phase Cl^- increases at high RH between 70-100 %

321 and thus increases the NH_4^+ concentration. The HCl/Cl^- is highly anticorrelated (r = -0.53) with NH_4^+

322 concentration in the presence of high RH (70-100 %), further supporting the view that HCl promotes the increase

323 in the particle fraction of NH_4^+ (49.5 %) with Cl^- (29.7 %) the primary anion.

324   We investigated the directions of local emission sources associated with concentration increases of NH_3,

325 NH_4^+, Cl^- and NH_x through bivariate polar graphs using the OpenAir software (Carslaw and Ropkins, 2012) at the

326 IGIA site. Figure 5 shows the bivariate polar plots of mean NH_3 (Fig. 5a), NH_4^+ (Fig. 5b), Cl^- (Fig. 5c), and total

327 NH_x (Fig. 5d) concentration for the observation period in relation to wind speed and wind direction. The 270-300º

328 sector dominated the wind direction at IGIA (Acharja et al., 2021). Figure 5a shows that the highest NH_3

329 concentration was associated with the winds coming from the east and southeast of the site, where it could have

330 been emitted from dairy farms, including animal houses, yards, and manure storage, as well as by the application

331 to the farmland of urea and other ammoniacal fertilizers, ammoniacal wastes and ruminant urine located at this

332 region (Hindustan Times, 2021; Leytem et al., 2018; Sherlock et al., 1994). Such sources of NH_3 volatilization

333 (Hristov et al., 2011; Laubach et al., 2013) can also explain the higher concentrations of total NH_4^+ (and, by

334 definition NH_x) for air coming from the southeast of the measurement site (Fig. 5b and d). This enhancement in

335 the southeast region is not only affected by emissions but also by meteorology and chemistry. Thus higher NH_3

336 concentration may also be due to the lack of turbulent mixing, which restricts the dilution of plumes from local

337 point sources at lower wind speeds (Ianniello et al., 2010). The bivariate polar plots of NH_4^+ (Fig. 5b) and Cl^-

338 (Fig. 5c) concentration point to the west direction as a principal source for thermodynamic partitioning of NH_3

339 and HCl to the condensed phase to form NH_4^+ and Cl^-. Two industrial sources are located in this direction: the

340 site is impacted by a cluster in northwest Delhi of industrial processes, such as steel pickling industries, and others

341 include metal finishing and electroplating, which are known to be vital HCl emitters (Acharja et al., 2021;

342 Jaiprakash et al., 2017). Near the source, abundant quantities of NH_3 may drive the partitioning of HCl to the

343 condensed phase resulting in high concentrations of NH_4^+ and Cl^- towards the west at lower wind speeds. Thus,

344 high NH_4^+ and Cl^- correspond to the lowest NH_3 concentration region (inverse relation), which can be observed

345 in Fig. 5a, b, and c, highlighting the importance of nearby HCl industrial sources in driving the particle fraction

346 of NH_4^+ and Cl^-.

347   To gain insight into the role of NH_4^+ in the neutralization of anions (SO_4^{2-}, NO_3^- and Cl^-), the aerosol

348   neutralization ratio (ANR) was calculated using the observed data. The ANR is defined as the equivalent ratio of

349   NH_4^+ to the sum of SO_4^{2-}, NO_3^- and Cl^- because these species represent the dominant cations and anions in $PM_{2.5}$,

350   respectively. Figure 6 demonstrates, on average, how well the charge balance works between Cl^-, NO_3^- and SO_4^{2-}

351   (in µeq m^{-3}) as the anions and NH_4^+ as the major cation (ANR close to unity), with Cl^- as the most significant

352   anion followed by NO_3^- and SO_4^{2-}. The mean $\pm 1\sigma$ ANR value for $PM_{2.5}$ during the observed period was 0.96 $\pm$

353   0.14. It ranges from a minimum of 0.35 $\pm$ 0.04 to a maximum of 2.31 $\pm$ 0.08. Higher values than unity may indicate

354   the presence of organic acids in the aerosol, which MARGA does not measure (Acharja et al., 2020). Also, high

355   standard error in Fig.6 indicates the possibility of uncertainties associated with the breakthrough of NH_3 spikes on

356   the denuder at high concentration (~ 1 %) (Stieger et al., 2019). However, the good charge balance indicates this

357   wasn't a major issue. There also were certain periods where low concentrations were observed of Cl^- and NO_3^-

358   (03-06 January 2018 and 16-17 January 2018) in Fig. 6. Comparing the model/obs for NH_3, NH_4^+ and total NH_x

359   during these periods provides some degree of validation of the model where sulfur chemistry dominates the

360   reaction with NH_3. Figure S4 (in the supplement) shows that model/obs indicates substantial variability which

361   appears to be overestimating NH_3 (model/obs >1) while underestimating total NH_4^+ (model/obs <1) on average

362   in the model.

3.3 Influence of HCl/Cl$^-$ chemistry in WRF-Chem

364   We further conducted three scenario simulations for the period 7-16 January 2018 (10 days) to explore the

365   potential impacts of the addition of anthropogenic chloride (HCl/Cl$^-$) emissions in the concentrations of NH_3,

366   NH_4^+ and total NH_x. We employ the HCl emissions from trash-burning activities in Delhi, as predicted by Sharma

367   et al. (2019) in our model set-up. We tested the three sensitivity experiments named: No HCl (0 mol km^{-2} h^{-1}),

368   Base Case HCl (3$\times$ Sharma et al., 2019; 24.8 mol km^{-2} h^{-1}), and 3$\times$Base HCl (74 mol km^{-2} h^{-1}) scenario, reflecting

369   adjustments which are consistent with the more recent upward adjustments in the amount of waste burned in

370   landfills by Chaudhary et al. (2021) and also to reflect additional industrial HCl sources not accounted for in the

371   inventory. Figure 7 presents the box-whiskers plots for secondary inorganic aerosols and trace gases from the

372   observations (MARGA), and those simulated by the model for the three sensitivity experiments. Daily mean $\pm 1\sigma$

373   values are summarized in Table 2 for three different model scenarios. As can be observed from Fig. 7(a-c),

374   increasing the HCl emissions (Fig. 7g) in the model partitions more NH_3 to the condensed phase due to its high

375   concentrations, reaching maximum mass loadings of NH_4^+ and Cl^- of 70 and 110 µg m^{-3}, respectively, in the

376   3$\times$Base HCl scenario, while increasing the total mean NH_x concentration by 15 µg m^{-3} compared to the No HCl

377   run presumably reflecting the longer residence time of NH_4^+ for near-surface air measurements.

378   The simulated NO_3^- concentration (Fig. 7e) generally exceeds the measurements in all three experiments;

379   since the main neutralizing species for NO_3^- is NH_4^+, it is controlled via the equilibrium between NO_3^-, HNO_3, and

380   NH_3, but also the competition with HCl for free NH_3. Simulated HNO_3 is significantly underestimated (by ~3 µg

381   m^{-3}) (Fig. 7h) by the model compared to the observations. As a consequence, the model suggests that NO_3^-

382   formation from gaseous NH_3 and HNO_3 cannot occur. The gas fraction of observed HNO_3 will be determined by

383   aerosol pH and liquid water content based on NH_3 and NO_3^- availability (Nenes et al., 2020). The over-prediction

384   of NH_3 concentration in the model compared with the observations generates more NO_3^- (and simultaneously

385   reduces HNO_3), with the total fraction of $HNO_3 + NO_3^-$ (THNO$_3$) concentration in the model also exceeding the

386   observed THNO$_3$, which is more strongly affected by reducing the NH$_3$ emissions in the model (Fig. S5 in the

387   Supplement). On average, THNO$_3$ reduced by only 0.38 µg m^{-3} in 3×Base HCl compared to the No HCl run. But

388   reducing NH$_3$ emissions by a factor of 3 (-3×NH$_3$_EMI) in the 3×Base HCl scenario reduced mean THNO$_3$ by a

389   further 4.71 µg m^{-3}. The extent of partitioning and accumulation of NH$_4$NO$_3$ depends on T, aerosol water, pH, as

390   well as NH$_3$ availability (Nenes et al., 2020). Our model simulations find that the presence of HCl/Cl$^-$ does not

391   significantly alter THNO$_3$ but that the excess NH$_3$ with missing chloride chemistry is a major contributor and will

392   lead to mismatches in the model between measured simulated gas and particulate matter concentrations.

393   The simulated SO$_4^{2-}$ concentration (Fig. 7f) was underestimated (by $\sim$ 7.5 µg m^{-3}), while gas-phase SO$_2$

394   Fig. 7i) was found to be overestimated by about 16 µg m^{-3} in all three experiments compared with the observations.

395   This may be caused by the fact that the drivers for typical sulfate production via OH or aqueous H$_2$O$_2$ oxidation

396   pathway are likely to be wrong in the model. The missing chemistry may underly this mismatch and requires

397   further sensitivity studies considering different SO$_2$ oxidation pathways. This requires further study, such as

398   scenario evaluation of altered SO$_2$ emissions in the model, to examine the main pathway(s) for SO$_2$ to SO$_4^{2-}$

399   conversion. Measurements of OH and other radicals in Delhi are currently lacking, making it difficult to constrain

400   the associated chemical schemes. To investigate the further impact of 3×Base HCl in the model, uptake of gaseous

401   NH$_3$ to form NH$_4^+$ and Cl$^-$ was analyzed via a strong correlation coefficient values of r = 0.84 for NH$_4^+$/NH$_x$ with

402   Cl$^-$ concentration, indicating a fraction of gas-to-particle conversion in the model correlates well with the Cl$^-$

403   concentration and was reasonably well simulated in the 3×Base HCl run.

404   **3.4 Comparison of the temporal variation in NH$_3$, NH$_4^+$, and NH$_x$ using WRF-Chem (HCl/Cl$^-$) and**
405   **MARGA**

406   **3.4.1 Diurnal variation**

407   Here, diurnal variations of monitored aerosol compounds and gases were analysed to investigate the gas-to-

408   particle conversion of NH$_3$ in the model. We analyzed the simulation results of the 3×Base HCl run**.** The diurnal

409   variations for NH$_3$ and NH$_4^+$ are controlled mainly by thermodynamic gas-to-particle partitioning, boundary layer

410   mixing, emission and deposition processes, along with vertical and horizontal advection (Meng et al., 2018).

411   Figure 8 (top) presents the diurnal variations of NH$_3$ and NH$_4^+$ (in µg m^{-3}) along with particulate NH$_4^+$, Cl$^-$, NO$_3^-$

412   , SO$_4^2$, SO$_2$, HCl, and HNO$_3$ concentrations (in µeq m^{-3}) measured (Fig. 8a (top)) and modeled (Fig. 8b (top))

413   along with its meteorological parameters such as T and RH (Fig. 8 (bottom)). We adopted diurnal variation in

414   emissions from Jena et al. (2021) based on boundary layer mixing. It can be seen in Fig. 8a (top and bottom) that

415   a much bigger peak in NH$_3$ concentration is observed in the daytime than the modeled (despite turbulence

416   differences), indeed suggesting a much stronger NH$_3$ in the middle of the day (11:00-01:00 h). As evaporation

417   proceeds mainly in the morning (08:00-12:00) getting warmer, the peak is near midday (11:00-13:00 h), rather

418   than in the afternoon (13:00-14:00 h) when warmest, similar to what was also observed in Sutton et al. (1998).

419   Indeed, the decreasing NH$_4^+$ and Cl$^-$ during the late morning (10:00 h) corresponds to the increasing NH$_3$ peak,

420   which reflects the fact that warming promotes the shift of aerosols to the gas phase. Ammonium decrease more

421   than NH$_3$ during the day, as this also evaporates to form NH$_3$. Similarly, Cl$^-$ evaporates during the day since the

422   HCl concentration increases. However, it can be seen that NO$_3^-$ and SO$_4^{2-}$ are slightly changed diurnally, inferring

423   longer range transport perhaps, whereas HCl and Cl$^-$ are from more local sources. The diurnal variability in gases

424   and aerosols in 3×Base HCl simulations in Fig. 8b (top) is primarily controlled by the planetary boundary layer

425   mixing, meteorology/dispersion, environment (T and RH in Fig. 8b (bottom)), and transport. So presumably,

426   maximum NH_3 at 08:00 h is due to limited turbulence/boundary layer, with dilution by mixing after 08:00 h.

427   However, the model is able to represent well the diurnal variation of NH_4^+ and Cl^- both in terms of amount and

428   pattern, which was not the case in the No HCl run where NH_4^+ was observed to be flat in Section 1. During the

429   hours of 09:00 and 11:00 h, when measured NH_3 rises, the model predicts a large decrease in NH_3, while during

430   19:00-23:00 h, when measured NH_3 decreases, the model predicts a large increase. Furthermore, the modeled HCl

431   and HNO_3 are very low compared to the measurements, whereas SO_2 concentration matches well with the

432   observations. It can be seen that NO_3^- and SO_4^{2-} are flat in the model. This highlights the need to develop accurate

433   diurnal variability in NH_3 emissions over this region.

434   Figure 9 presents the differences in diurnal variation of mean NH_3 (Fig. 9a), NH_4^+ (Fig. 9b), and total

435   NH_x (Fig. 9c) concentration for the three sensitivity experiments. While the simulated NH_3 concentrations

436   decrease in the 3×Base HCl compared to the No HCl and Base Case HCl run (Table 2), none of the model

437   experiments capture the diurnal cycle of NH_3. Higher levels of observed NH_3 during daytime and modeled NH_3

438   during night-time highlight the need to improve diurnal variability in NH_3 emissions over this region based on the

439   nature and strength of the actual sources. Between the No HCl and the 3xBase HCl run, the NMB for NH_3 reduced

440   from 1.38 to 1.13, and NMB for NH_4^+ systematically improved from -0.61 to -0.03. In contrast, NMB for total

441   NH_x increased from 0.12 to 0.39. Table 3 summarizes the statistical indicators for the three sensitivity

442   experiments. An increase in HCl emissions in the 3×Base HCl leads to a higher mass concentration of NH_4^+ and

443   Cl^-, which also increases total mean NH_x concentration by 22.4 µg m^{-3}, presumably reflecting the longer

444   atmospheric lifetime of NH_4^+ compared with NH_3. We find consistent high bias in all the simulations for NH_3,

445   which is highest during the early morning and at night-time.

446   **3.4.2 Variation of daily means**

447   Figure S6 in the Supplement illustrates a time-series graph that compares daily mean NH_3 (Fig. S6a), NH_4^+ (Fig.

448   S6b), and total NH_x concentrations (Fig. S6c) for the three sensitivity experiments, and Table 2 shows the mean

449   ± 1σ of these variables. The results show that compared to the No HCl run, NH_3 mean concentrations decreased

450   by 2 µg m^{-3} in the Base Case HCl and decreased by a further 3.2 µg m^{-3} in the 3×Base HCl run. On the contrary,

451   NH_4^+ mean concentration increases in the Base Case HCl by 7.5 µg m^{-3} and further increases by 13.1 µg m^{-3}

452   (3×Base HCl). This decrease in NH_3 is associated with the enhanced gas-to-particle conversion of NH_3 to NH_4^+.

453   Associated with these changes, total mean NH_x also increased by 5.5 and 9.8 µg m^{-3} in the Base Case HCl and

454   3×Base HCl, respectively, compared to the No HCl. This is likely due to associated increases in the atmospheric

455   lifetime of NH_x with respect to deposition as the partitioning shifted from the faster depositing gas phase to the

456   aerosol phase. The lifetime of NH_3 is very short, a few hours, while that of NH_4^+ is 1 to 15 days (Aneja et al.,

457   1998; Nair and Yu, 2020; Pawar et al., 2021; Wang et al., 2020a).

458   To understand further the overestimation of total NH_x by the model, we performed a sensitivity test with

459   the HCl emissions that led to the best model/obs comparison (3×Base HCl emissions) by additionally reducing

460   NH_3 emissions by a factor of 3 (-3×NH3_EMI). Figure 10 shows the ratio of model/obs for NH_3 (Fig. 10a), NH_4^+

461   (Fig. 10b) and total NH_x (Fig. 10c) concentration. It can be seen that the model-measurement agreement improves

462   significantly (model/obs closer to 1) after reducing NH_3 emissions for all three metrics. -3×NH3_EMI would

463   reduce the mean NH_3, NH_4^+, and total NH_x concentration by ~8.1 µg m^{-3}, 3.2 µg m^{-3}, and 11.3 µg m^{-3}, respectively,

464   compared to the 3×Base HCl run. Even though reducing NH$_3$ emissions, it is still sufficient to react rapidly with

465   the varying HCl in the sensitivity experiments contributing to an increase in NH$_4^+$. As can be seen in Fig. 10b,

466   initially, NH$_4^+$ is somewhat lower, but it increases later and matches the 3×Base HCl run. This suggests that NH$_4^+$

467   formation in the model is more sensitive to changes in HCl than changes in NH$_3$ emission, while total NH$_x$ agrees

468   well by reducing the NH$_3$ emissions. In general, CTMs have higher NH$_3$ concentration than observations, further

469   supporting models having too much NH$_3$. A few factors might contribute to the model discrepancies for NH$_3$:

470   there are uncertainties in the emission inventory of the bottom-up approach of NH$_3$, and the model does not

471   currently include the bidirectional exchange of NH$_3$ with surfaces, such as dew and fog water. Also model does

472   not have accurate industrial sources of HCl emission. Diurnal emission profiles are uncertainty for both NH$_3$ and

473   HCl. Furthermore, gas-to-particle partitioning associated with SO$_2$ oxidation pathways in the model is not correct

474   at present.

4. Conclusions

476   In this study, we have evaluated for the first time in South Asia the performance of a chemical transport model

477   (WRF-Chem) in modeling NH$_3$, NH$_4^+$, and total NH$_x$, by comparing against the WiFEX measurements

478   (MARGA). The model predicted average NH$_3$ and NH$_4^+$ mass loadings of 56.7 ± 14.3 and 14.7 ± 4.9 µg m^{-3}

479   respectively, whereas the measurements depicted 28.2 ± 12.4 and 36.9 ± 15.1 µg m^{-3}, respectively, in the diurnal

480   concentration. Simulated NH$_3$ concentrations peaked with bimodal variation, though observations showed a

481   daytime rise around 12:00-13:00 h. Ammonia peaks during the daytime suggested that the NH$_4^+$ volatilization is

482   causing its rise. Also, the role of fog and dew in enhancing NH$_3$ pulses requires further attention, and it is currently

483   not incorporated into the model. In daily means, we find NH$_3$ is significantly overestimated by the model, NH$_4^+$

484   was underestimated while simulated total NH$_x$ agreed well with the measurement, indicating incorrect gas-to-

485   particle partitioning along with missing chemical process may impacts this mismatch in the model. The ability of

486   the model to accurately describe the gas-to-particle partitioning of the MARGA was evaluated by the fraction of

487   total NH$_x$ (= NH$_3$ + NH$_4^+$) in the particulate phase (NH$_4^+$/NH$_x$). A strong relation of MARGA NH$_4^+$/NH$_x$ was

488   observed with dominant anion (Cl$^-$) (r = 0.79), whereas the standard model showed a strong correlation between

489   NH$_4^+$/NH$_x$ with dominant anion (SO$_4^{2-}$) (r = 0.77), pointing to the missing chloride (HCl/Cl$^-$) chemistry in the

490   model. Measured HCl/Cl$^-$ correlated highly (r = -0.53) with the NH$_4^+$ levels, in the presence high RH (70-100 %),

491   indicated HCl promoting the increase in the particle fraction of NH$_4^+$ (49.5 %) with Cl$^-$ (29.7 %) as the primary

492   anion. On average, the measured aerosol neutralization ratio (ANR) was close to unity (0.96) with Cl$^-$ the most

493   significant anion followed by NO$_3^-$ and SO$_4^{2-}$.

494   We further incorporated HCl/Cl$^-$ emissions in the model and conducted three sensitivity experiments of

495   varying HCl emissions, named as No HCl (0 mol km^{-2} h^{-1}), Base Case HCl (3× Sharma et al., 2019; 24.8 mol km$^-$

496   ^{2} h^{-1}) and 3×Base HCl (74 mol km^{-2} h^{-1}) run. The revised model shows that HCl emissions in the model were

497   partitioning more NH$_3$ to the condensed phase, due to its high concentrations, reaching maximum mass loadings

498   of NH$_4^+$ and Cl$^-$ of 70 and 110 µg m^{-3} µg m^{-3}, respectively, in the 3×Base HCl run, while increasing the total mean

499   NH$_x$ concentration by 15 µg m^{-3} compared to the No HCl run. 3×Base HCl was able to represent well the diurnal

500   variation of NH$_4^+$ and Cl$^-$ both in terms of amount and pattern. The NMB for NH$_3$ was found to be reduced from

501   1.38 to 1.13 while NMB for NH$_4^+$ systematically improved from -0.61 to -0.03 in 3×Base HCl. By contrast, NMB

502   for NH$_x$ increased from 0.12 to 0.39, respectively, for the No HCl and 3×Base HCl simulations. Our modeling

503 results suggest reducing NH_3 emissions by a factor of 3 (-3×NH_3_EMI) in the 3×Base HCl was successful in

504 reducing the mean NH_3, NH_4^+ and total NH_x concentration by ~ 8.1 µg m^{-3}, 3.2 µg m^{-3}, and 11.3 µg m^{-3},

505 respectively, compared to the 3×Base HCl. We find excess NH_3 along with longer lifetime of NH_4^+ may act as a

506 controlling driver for NH_x overestimation in the model.

507   Hence, in the future, it is necessary to evaluate the impact of the addition of correct industrial sources of

508 HCl emission along with appropriate emissions of NH_3 and their diurnal variability, and improvements to the

509 chemistry in model are suggested to address the challenges of simulating NH_3 as a contributor to particulate

510 matter. Additionally, it is required to understand different SO_2 oxidation pathways in the model. To our

511 knowledge, this is the first study to qualitatively examine the influence of HCl/Cl$^-$ chemistry in WRF-Chem in

512 determining the fraction of NH_4^+/NH_x. The present study suggests that the bias in NH_x could be reduced by

513 including both the accurate HCl and NH_3 emissions in the model. Developing the appropriate NH_3 emissions

514 using country-specific emission inventories, which are currently under development as part of the Global

515 Challenges Research Fund (GCRF), South Asian Nitrogen Hub (SANH). Also, there is potential to develop top-

516 down constraints on NH_3 emissions by taking inference from the satellite, model, and ground-based observations.

Data availability

518 The 0.1° × 0.1° emission grid maps can be downloaded from the EDGAR website on

519 https://edgar.jrc.ec.europa.eu/htap_v2/index.php?SECURE=_123 per year per sector. Gridded emissions in t y^{-1}

520 on a 0.1° × 0.1° for HCl emissions can be downloaded from Mendeley data: http://dx.doi.org/10.

521 17632/546t9249bv.1. The model data is available at Aditya, Indian Institute of Tropical Meteorology

522 (IITM) super-computer and can be provided upon request to the corresponding author. The observational and

523 meteorological data of WiFEX are available by contacting the corresponding author.

Author contributions

525 SDG designed the research; PVP performed the WRF-Chem model simulations and led the analysis; PA and RK

526 contributed to data collection and its quality control and assurance; GG, RK, and PG helped with the model set

527 up; PVP and SDG wrote the paper with contributions from all co-authors.

Competing interests

529 The authors declare that they have no conflict of interest.

Acknowledgments

531 We thank the Director, IITM, for his continuous support and encouragement. IITM is funded by the Ministry of

532 Earth Sciences (MoES), Government of India. We wish to thank the MoES for supporting the WiFEX campaign.

533 The lead author's fellowship was supported by the National Supercomputing Mission (NSM) program grant at C-

534 DAC, and Ph.D. fees are covered by the Natural Environment Research Council (NERC) of UK Research and

Innovation (UKRI)-Global Challenges Research Fund (GCRF), South Asian Nitrogen Hub (SANH), and we are grateful to the Executive Director and the Director-General of C-DAC and the SANH Director and Chair of the Executive Board. We acknowledge the availability of CPCB-NO_x, NO_2, and O_3 data from the CPCB web portal (https://app.cpcbccr.com/ccr, last access: 1 December 2021). We wish to acknowledge the National Center for Atmospheric Research is sponsored by the National Science Foundation.

5. References

Acharja, P., Ali, K., Trivedi, D. K., Safai, P. D., Ghude, S., Prabhakaran, T. and Rajeevan, M.: Characterization of atmospheric trace gases and water soluble inorganic chemical ions of PM1 and PM2.5 at Indira Gandhi International Airport, New Delhi during 2017–18 winter, Sci. Total Environ., 729, 138800, doi:10.1016/j.scitotenv.2020.138800, 2020.

Acharja, P., Ali, K., Ghude, S. D., Sinha, V., Sinha, B., Kulkarni, R., Gultepe, I. and Nair, M.: Chemosphere Enhanced secondary aerosol formation driven by excess ammonia during fog episodes, Chemosphere, 289(November 2021), 133155, doi:10.1016/j.chemosphere.2021.133155, 2021.

Ali, K., Acharja, P., Trivedi, D. K., Kulkarni, R., Pithani, P., Safai, P. D., Chate, D. M., Ghude, S., Jenamani, R. K. and Rajeevan, M.: Characterization and source identification of PM 2.5 and its chemical and carbonaceous constituents during Winter Fog Experiment 2015–16 at Indira Gandhi International Airport, Delhi, Sci. Total Environ., 662, 687–696, doi:10.1016/j.scitotenv.2019.01.285, 2019.

Aneja, V. P., Murray, G. C. and Southerland, J.: Atmospheric nitrogen compounds: Emissions, transport, transformation, deposition, and assessment, EM Air Waste Manag. Assoc. Mag. Environ. Manag., 22–25, 1998.

Behera, S. N., Sharma, M., Aneja, V. P. and Balasubramanian, R.: Ammonia in the atmosphere: a review on emission sources, atmospheric chemistry and deposition on terrestrial bodies, Environ. Sci. Pollut. Res., 20(11), 8092–8131, doi:10.1007/s11356-013-2051-9, 2013.

Bucaram, C. J. and Bowman, F. M.: Wrf-chem modeling of summertime air pollution in the northern great plains: Chemistry and aerosol mechanism intercomparison, Atmosphere (Basel)., 12(9), doi:10.3390/atmos12091121, 2021.

Carslaw, D. C. and Ropkins, K.: Openair - An r package for air quality data analysis, Environ. Model. Softw., 27–28(July 2019), 52–61, doi:10.1016/j.envsoft.2011.09.008, 2012.

Chaudhary, P., Garg, S., George, T., Shabin, M., Saha, S., Subodh, S. and Sinha, B.: Underreporting and open burning – the two largest challenges for sustainable waste management in India, Resour. Conserv. Recycl., 175, 105865, doi:https://doi.org/10.1016/j.resconrec.2021.105865, 2021.

Chen, Y., Wang, Y., Nenes, A., Wild, O., Song, S., Hu, D., Liu, D., He, J., Hildebrandt Ruiz, L., Apte, J. S., Gunthe, S. S. and Liu, P.: Ammonium Chloride Associated Aerosol Liquid Water Enhances Haze in Delhi, India, Environ. Sci. Technol., 56(11), 7163–7173, doi:10.1021/acs.est.2c00650, 2022.

Clarisse, L., Clerbaux, C., Dentener, F., Hurtmans, D. and Coheur, P. F.: Global ammonia distribution derived from infrared satellite observations, Nat. Geosci., 2(7), 479–483, doi:10.1038/ngeo551, 2009.

Clarisse, L., Shephard, M. W., Dentener, F., Hurtmans, D., Cady-Pereira, K., Karagulian, F., Van Damme, M., Clerbaux, C. and Coheur, P. F.: Satellite monitoring of ammonia: A case study of the San Joaquin Valley, J. Geophys. Res. Atmos., 115(13), 1–15, doi:10.1029/2009JD013291, 2010.

CPCB: Annual Report 2014-15., 2014.

574   CPCB: Annual Report Annual Report., 2020.

575   Van Damme, M., Clarisse, L., Whitburn, S., Hadji-Lazaro, J., Hurtmans, D., Clerbaux, C. and Coheur, P. F.:

576   Industrial and agricultural ammonia point sources exposed, Nature, 564(7734), 99–103, doi:10.1038/s41586-018-

577   0747-1, 2018.

578   Datta, A., Sharma, S. K., Harit, R. C., Kumar, V., Mandal, T. K. and Pathak, H.: Ammonia emission from

579   subtropical crop land area in india, Asia-Pacific J. Atmos. Sci., 48(3), 275–281, doi:10.1007/s13143-012-0027-1,

580   2012.

581   Duan, X., Yan, Y., Peng, L., Xie, K., Hu, D., Li, R. and Wang, C.: Role of ammonia in secondary inorganic

582   aerosols formation at an ammonia-rich city in winter in north China: A comparative study among industry, urban,

583   and rural sites, Environ. Pollut., 291(May), 118151, doi:10.1016/j.envpol.2021.118151, 2021.

584   Ellis, R. A., Murphy, J. G., Markovic, M. Z., Vandenboer, T. C., Makar, P. A., Brook, J. and Mihele, C.: The

585   influence of gas-particle partitioning and surface-atmosphere exchange on ammonia during BAQS-Met, Atmos.

586   Chem. Phys., 11(1), 133–145, doi:10.5194/acp-11-133-2011, 2011.

587   FINNv1.5: FINN Data, [online] Available from: http://bai.acom.ucar.edu/Data/fire/ (Accessed 15 April 2019),

588   n.d.

589   Freitas, S. R., Longo, K. M., Chatfield, R., Latham, D., Silva Dias, M. A. F., Andreae, M. O., Prins, E., Santos, J.

590   C., Gielow, R. and Carvalho Jr., J. A.: Including the sub-grid scale plume rise of vegetation fires in low resolution

591   atmospheric transport models, Atmos. Chem. Phys., 7(13), 3385–3398, doi:10.5194/acp-7-3385-2007, 2007.

592   Georgiou, G. K., Christoudias, T., Proestos, Y., Kushta, J., Hadjinicolaou, P. and Lelieveld, J.: Air quality

593   modelling in the summer over the eastern Mediterranean using WRF-Chem: chemistry and aerosol mechanism

594   intercomparison, Atmos. Chem. Phys., 18(3), 1555–1571, doi:10.5194/acp-18-1555-2018, 2018.

595   Ghude, S., Kumar, R., Jena, C., Debnath, S., Kulkarni, R., Alessandrini, S., Biswas, M., Kulkrani, S., Pithani, P.,

596   Kelkar, S., Sajjan, V., Chate, D., Soni, V., Singh, S., Nanjundiah, R. and Rajeevan, M.: Evaluation of PM2.5

597   Forecast using Chemical Data Assimilation in the WRF-Chem Model: A Novel Initiative Under the Ministry of

598   Earth   Sciences   Air   Quality   Early   Warning   System   for   Delhi,   India,   Curr.   Sci.,   118,

599   doi:10.18520/cs/v118/i11/1803-1815, 2020.

600   Ghude, S. D.: Premature mortality in India due to PM2.5 and ozone exposure, Geophys. Res. Lett., 1–8,

601   doi:10.1002/2013GL058740.Received, 2016.

602   Ghude, S. D., Fadnavis, S., Beig, G., Polade, S. D. and van der A, R. J.: Detection of surface emission hot spots,

603   trends, and seasonal cycle from satellite-retrieved NO $_2$ over India, J. Geophys. Res., 113(D20), D20305,

604   doi:10.1029/2007JD009615, 2008a.

605   Ghude, S. D., Jain, S. L., Arya, B. C., Beig, G., Ahammed, Y. N., Kumar, A. and Tyagi, B.: Ozone in ambient air

606   at a tropical megacity, Delhi: Characteristics, trends and cumulative ozone exposure indices, J. Atmos. Chem.,

607   60(3), 237–252, doi:10.1007/s10874-009-9119-4, 2008b.

608   Ghude, S. D., Van der A, R. J., Beig, G., Fadnavis, S. and Polade, S. D.: Satellite derived trends in NO2 over the

609   major global hotspot regions during the past decade and their inter-comparison, Environ. Pollut., 157(6), 1873–

610   1878, doi:10.1016/j.envpol.2009.01.013, 2009.

611   Ghude, S. D., Lal, D. M., Beig, G., van der A, R. and Sable, D.: Rain-Induced Soil NO $_x$ Emission From India

612   During the Onset of the Summer Monsoon: A Satellite Perspective, J. Geophys. Res., 115(D16), D16304,

613   doi:10.1029/2009JD013367, 2010.

614   Ghude, S. D., Pfister, G. G., Jena, C. K., Emmons, L. K., Kumar, R. and van der A, R. J.: Satellite constraints of

615   Nitrogen Oxide (NOX) emissions from India based on OMI observations and WRF-Chem simulations, Geophys.

616   Res. Lett., 40(x), 423–428, doi:10.1029/2012gl053926, 2012.

617   Ghude, S. D., Kulkarni, S. H., Jena, C., Pfister, G. G., Beig, G., Fadnavis, S. and Van Der, R. J.: Application of

618   satellite observations for identifying regions of dominant sources of nitrogen oxides over the indian subcontinent,

619   J. Geophys. Res. Atmos., 118(2), 1075–1089, doi:10.1029/2012JD017811, 2013.

620   Ghude, S. D., Bhat, G. S., Prabhakaran, T., Jenamani, R. K., Chate, D. M., Safai, P. D., Karipot, A. K., Konwar,

621   M., Pithani, P., Sinha, V., Rao, P. S. P., Dixit, S. A., Tiwari, S., Todekar, K., Varpe, S., Srivastava, A. K., Bisht,

622   D. S., Murugavel, P., Ali, K., Mina, U., Dharua, M., Rao, Y. J., Padmakumari, B., Hazra, A., Nigam, N., Shende,

623   U., Lal, D. M., Chandra, B. P., Mishra, A. K., Kumar, A., Hakkim, H., Pawar, H., Acharja, P., Kulkarni, R.,

624   Subharthi, C., Balaji, B., Varghese, M., Bera, S. and Rajeevan, M.: Winter fog experiment over the Indo-Gangetic

625   plains of India, Curr. Sci., 112(4), doi:10.18520/cs/v112/i04/767-784, 2017.

626   Ginoux, P., Chin, M., Tegen, I., Goddard, T. and In-, G.: Sources and distribution of dust aerosols simulated with

627   the GOCART model, J. Geophys. Res., 106, 20255–20273, doi:https://doi.org/10.1029/2000JD000053, 2001.

628   Gu, B., Zhang, L., Dingenen, R. Van, Vieno, M., Grinsven, H. J. Van, Zhang, X., Zhang, S., Chen, Y., Wang, S.,

629   Ren, C., Rao, S., Holland, M., Winiwarter, W., Chen, D., Xu, J. and Sutton, M. A.: Abating ammonia is more

630   cost-effective than nitrogen oxides for mitigating PM2.5 air pollution, Science (80-.)., 374(6568), 758–762,

631   doi:10.1126/science.abf8623, 2021.

632   Guenther, A., Karl, T., Harley, P., Wiedinmyer, C., Palmer, P. I. and Geron, C.: Estimates of global terrestrial

633   isoprene emissions using MEGAN (Model of Emissions of Gases and Aerosols from Nature), Atmos. Chem.

634   Phys., 6(11), 3181–3210, doi:10.5194/acp-6-3181-2006, 2006.

635   Gunthe, S. S., Liu, P., Panda, U., Raj, S. S., Sharma, A., Darbyshire, E., Reyes-Villegas, E., Allan, J., Chen, Y.,

636   Wang, X., Song, S., Pöhlker, M. L., Shi, L., Wang, Y., Kommula, S. M., Liu, T., Ravikrishna, R., McFiggans, G.,

637   Mickley, L. J., Martin, S. T., Pöschl, U., Andreae, M. O. and Coe, H.: Enhanced aerosol particle growth sustained

638   by high continental chlorine emission in India, Nat. Geosci., 14(2), 77–84, doi:10.1038/s41561-020-00677-x,

639   2021.

640   Gupta, M. and Mohan, M.: Validation of WRF/Chem model and sensitivity of chemical mechanisms to ozone

641   simulation over megacity Delhi, Atmos. Environ., 122, 220–229, doi:10.1016/j.atmosenv.2015.09.039, 2015.

642   Hindustan Times: 66 dairies, six dyeing units shut down in east Delhi, Hindustan Times, 6th July, 2021.

643   Hristov, A. N., Hanigan, M., Cole, A., Todd, R., McAllister, T. A., Ndegwa, P. M. and Rotz, A.: Review:

644   Ammonia emissions from dairy farms and beef feedlots, Can. J. Anim. Sci., 91(1), 1–35, doi:10.4141/CJAS10034,

645   2011.

646   Huang, X., Song, Y., Li, M., Li, J., Huo, Q., Cai, X., Zhu, T., Hu, M. and Zhang, H.: A high-resolution ammonia

647   emission inventory in China, Global Biogeochem. Cycles, 26(1), 1–14, doi:10.1029/2011GB004161, 2012.

648   Ianniello, A., Spataro, F., Esposito, G., Allegrini, I., Rantica, E., Ancora, M. P., Hu, M. and Zhu, T.: Occurrence

649   of gas phase ammonia in the area of Beijing (China), Atmos. Chem. Phys., 10(19), 9487–9503, doi:10.5194/acp-

650   10-9487-2010, 2010.

651   Ianniello, A., Spataro, F., Esposito, G., Allegrini, I., Hu, M. and Zhu, T.: Chemical characteristics of inorganic

652   ammonium salts in PM2.5 in the atmosphere of Beijing (China), Atmos. Chem. Phys., 11(21), 10803–10822,

653   doi:10.5194/acp-11-10803-2011, 2011.

Jaiprakash, Singhai, A., Habib, G., Raman, R. S. and Gupta, T.: Chemical characterization of PM1.0 aerosol in Delhi and source apportionment using positive matrix factorization, Environ. Sci. Pollut. Res., 24(1), 445–462, doi:10.1007/s11356-016-7708-8, 2017.

Jena, C., Ghude, S., Kulkarni, R., Debnath, S., Kumar, R., Soni, V. K., Acharja, P., Kulkarni, S., Khare, M., Kaginalkar, A., Chate, D., Ali, K., Nanjundiah, R. and Rajeevan, M.: Evaluating the sensitivity of fine particulate matter (PM$_{2.5}$) simulations to chemical mechanism in Delhi, Atmos. Chem. Phys. Discuss., (3), 1–28, doi:10.5194/acp-2020-673, 2020.

Jena, C., Ghude, S. D., Kumar, R., Debnath, S., Govardhan, G., Soni, V. K., Kulkarni, S. H., Beig, G., Nanjundiah, R. S. and Rajeevan, M.: Performance of high resolution (400 m) PM2.5 forecast over Delhi, Sci. Rep., 11(1), 1–9, doi:10.1038/s41598-021-83467-8, 2021.

Knote, C., Hodzic, A. and Jimenez, J. L.: The effect of dry and wet deposition of condensable vapors on secondary organic aerosols concentrations over the continental US, Atmos. Chem. Phys., 15(1), 1–18, doi:10.5194/acp-15-1-2015, 2015.

Kulkarni, S. H., Ghude, S. D., Jena, C., Karumuri, R. K., Sinha, B., Sinha, V., Kumar, R., Soni, V. K. and Khare, M.: How Much Does Large-Scale Crop Residue Burning Affect the Air Quality in Delhi?, Environ. Sci. Technol., 54(8), 4790–4799, doi:10.1021/acs.est.0c00329, 2020.

Kumar, A., Hakkim, H., Ghude, S. D. and Sinha, V.: Probing wintertime air pollution sources in the Indo-Gangetic Plain through 52 hydrocarbons measured rarely at Delhi & Mohali, Sci. Total Environ., 801, 149711, doi:https://doi.org/10.1016/j.scitotenv.2021.149711, 2021.

Kumar, R., Barth, M. C., Pfister, G. G., Delle Monache, L., Lamarque, J. F., Archer-Nicholls, S., Tilmes, S., Ghude, S. D., Wiedinmyer, C., Naja, M. and Walters, S.: How Will Air Quality Change in South Asia by 2050?, J. Geophys. Res. Atmos., 123(3), 1840–1864, doi:10.1002/2017JD027357, 2018.

Kumar, R., Ghude, S. D., Biswas, M., Jena, C., Alessandrini, S., Debnath, S., Kulkarni, S., Sperati, S., Soni, V. K., Nanjundiah, R. S. and Rajeevan, M.: Enhancing Accuracy of Air Quality and Temperature Forecasts During Paddy Crop Residue Burning Season in Delhi Via Chemical Data Assimilation, J. Geophys. Res. Atmos., 125(17), 1–16, doi:10.1029/2020JD033019, 2020.

Kuttippurath, J., Singh, A., Dash, S. P., Mallick, N., Clerbaux, C., Van Damme, M., Clarisse, L., Coheur, P. F., Raj, S., Abbhishek, K. and Varikoden, H.: Record high levels of atmospheric ammonia over India: Spatial and temporal analyses, Sci. Total Environ., 740, 139986, doi:10.1016/j.scitotenv.2020.139986, 2020.

Lan, Z., Lin, W., Pu, W. and Ma, Z.: Measurement report: Exploring NH3 behavior in urban and suburban Beijing: Comparison and implications, Atmos. Chem. Phys., 21(6), 4561–4573, doi:10.5194/acp-21-4561-2021, 2021.

Laubach, J., Taghizadeh-Toosi, A., Gibbs, S. J., Sherlock, R. R., Kelliher, F. M. and Grover, S. P. P.: Ammonia emissions from cattle urine and dung excreted on pasture, Biogeosciences, 10(1), 327–338, doi:10.5194/bg-10-327-2013, 2013.

Leytem, A. B., Bjorneberg, D. L., Rotz, C. A., Moraes, L. E., Kebreab, E. and Dungan, R. S.: Ammonia emissions from dairy lagoons in the western U.S., Trans. ASABE, 61(3), 1001–1015, doi:10.13031/trans.12646, 2018.

Li, L., Chen, Z. M., Zhang, Y. H., Zhu, T., Li, S., Li, H. J., Zhu, L. H. and Xu, B. Y.: Heterogeneous oxidation of sulfur dioxide by ozone on the surface of sodium chloride and its mixtures with other components, J. Geophys. Res. Atmos., 112(18), 1–13, doi:10.1029/2006JD008207, 2007.

Makkonen, U., Virkkula, A., Mäntykenttä, J., Hakola, H., Keronen, P., Vakkari, V. and Aalto, P. P.: Semi-

continuous gas and inorganic aerosol measurements at a Finnish urban site: comparisons with filters, nitrogen in aerosol and gas phases, and aerosol acidity, Atmos. Chem. Phys., 12(12), 5617–5631, doi:10.5194/acp-12-5617-2012, 2012.

Mandal, T. K., Saxena, M., Rohtash, Sharma, S. K., Gupta, N. C., Kumar, M. and Saraswati: Characteristics of ambient ammonia over Delhi, India, Meteorol. Atmos. Phys., 124(1–2), 67–82, doi:10.1007/s00703-013-0299-8, 2013.

Meng, Z., Xu, X., Lin, W., Ge, B., Xie, Y., Song, B., Jia, S., Zhang, R., Peng, W., Wang, Y., Cheng, H., Yang, W. and Zhao, H.: Role of ambient ammonia in particulate ammonium formation at a rural site in the North China Plain, Atmos. Chem. Phys., 18(1), 167–184, doi:10.5194/acp-18-167-2018, 2018.

Metzger, S., Mihalopoulos, N. and Lelieveld, J.: Importance of mineral cations and organics in gas-aerosol partitioning of reactive nitrogen compounds: Case study based on MINOS results, Atmos. Chem. Phys., 6(9), 2549–2567, doi:10.5194/acp-6-2549-2006, 2006.

Móring, A., Hooda, S., Raghuram, N., Adhya, T. K., Ahmad, A., Bandyopadhyay, S. K., Barsby, T., Beig, G., Bentley, A. R., Bhatia, A., Dragosits, U., Drewer, J., Foulkes, J., Ghude, S. D., Gupta, R., Jain, N., Kumar, D., Kumar, R. M., Ladha, J. K., Mandal, P. K., Neeraja, C. N., Pandey, R., Pathak, H., Pawar, P., Pellny, T. K., Poole, P., Price, A., Rao, D. L. N., Reay, D. S., Singh, N. K., Sinha, S. K., Srivastava, R. K., Shewry, P., Smith, J., Steadman, C. E., Subrahmanyam, D., Surekha, K., Venkatesh, K., Varinderpal-Singh, Uwizeye, A., Vieno, M. and Sutton, M. A.: Nitrogen Challenges and Opportunities for Agricultural and Environmental Science in India, Front. Sustain. Food Syst., 5, 13, doi:10.3389/fsufs.2021.505347, 2021.

Nair, A. A. and Yu, F.: Quantification of atmospheric ammonia concentrations: A review of its measurement and modeling, Atmosphere (Basel)., 11(10), doi:10.3390/atmos11101092, 2020.

Nenes, A., Pandis, S. N., Weber, R. J. and Russell, A.: Aerosol pH and liquid water content determine when particulate matter is sensitive to ammonia and nitrate availability, Atmos. Chem. Phys., 20(5), 3249–3258, doi:10.5194/acp-20-3249-2020, 2020.

NIVDANGE, S., Jena, C. and Pawar, P.: Nationwide CoViD-19 lockdown impact on air quality in India, MAUSAM, 73(1), 115–128, doi:10.54302/mausam.v73i1.1475, 2022.

Pawar, P. V., Ghude, S. D., Jena, C., Móring, A., Sutton, M. A., Kulkarni, S., Lal, D. M., Surendran, D., Van Damme, M., Clarisse, L., Coheur, P.-F., Liu, X., Govardhan, G., Xu, W., Jiang, J. and Adhya, T. K.: Analysis of atmospheric ammonia over South and East Asia based on the MOZART-4 model and its comparison with satellite and surface observations, Atmos. Chem. Phys., 21(8), 6389–6409, doi:10.5194/acp-21-6389-2021, 2021.

Pinder, R. W., Adams, P. J. and Pandis, S. N.: Ammonia Emission Controls as a Cost-Effective Strategy for Reducing Atmospheric Particulate Matter in the Eastern United States, Environ. Sci. Technol., 41(2), 380–386, doi:10.1021/es060379a, 2007.

Pinder, R. W., Gilliland, A. B. and Dennis, R. L.: Environmental impact of atmospheric NH3 emissions under present and future conditions in the eastern United States, Geophys. Res. Lett., 35(12), doi:10.1029/2008GL033732, 2008.

Pollution, C. and Board, C.: Guidelines for Manual Sampling & Analyses., 2011.

Saraswati, George, M. P., Sharma, S. K., Mandal, T. K. and Kotnala, R. K.: Simultaneous Measurements of Ambient NH 3 and Its Relationship with Other Trace Gases, PM 2.5 and Meteorological Parameters over Delhi, India, Mapan - J. Metrol. Soc. India, 34(1), 55–69, doi:10.1007/s12647-018-0286-0, 2019.

734 Seinfeld, J. H. and Pandis, S. N.: Atmospheric chemistry and physics : from air pollution to climate change., n.d.

735 Seinfeld, J. H., Bretherton, C., Carslaw, K. S., Coe, H., DeMott, P. J., Dunlea, E. J., Feingold, G., Ghan, S.,

736 Guenther, A. B., Kahn, R., Kraucunas, I., Kreidenweis, S. M., Molina, M. J., Nenes, A., Penner, J. E., Prather, K.

737 A., Ramanathan, V., Ramaswamy, V., Rasch, P. J., Ravishankara, A. R., Rosenfeld, D., Stephens, G. and Wood,

738 R.: Improving our fundamental understanding of the role of aerosol–cloud interactions in the climate system, Proc.

739 Natl. Acad. Sci. U. S. A., 113(21), 5781, 2016.

740 Sha, T., Ma, X., Jia, H., Tian, R., Chang, Y., Cao, F. and Zhang, Y.: Aerosol chemical component: Simulations

741 with WRF-Chem and comparison with observations in Nanjing, Atmos. Environ., 218(June), 116982,

742 doi:10.1016/j.atmosenv.2019.116982, 2019.

743 Sharma, C., Tiwari, M. K. and Pathak, H.: Estimates of emission and deposition of reactive nitrogenous species

744 for India, Curr. Sci., 94(11), 1439–1446, 2008.

745 Sharma, G., Sinha, B., Pallavi, Hakkim, H., Chandra, B. P., Kumar, A. and Sinha, V.: Gridded Emissions of CO,

746 NOx, SO2, CO2, NH3, HCl, CH4, PM2.5, PM10, BC, and NMVOC from Open Municipal Waste Burning in

747 India, Environ. Sci. Technol., 53(9), 4765–4774, doi:10.1021/acs.est.8b07076, 2019.

748 Sharma, S. K., Saxena, M., Saud, T., Korpole, S. and Mandal, T. K.: Measurement of NH3, NO, NO2 and related

749 particulates at urban sites of indo gangetic plain (IGP) of India, J. Sci. Ind. Res. (India)., 71(5), 360–362, 2012.

750 Sharma, S. K., Harit, R. C., Kumar, V., Mandal, T. K. and Pathak, H.: Ammonia Emission from Rice-Wheat

751 Cropping System in Subtropical Soil of India, Agric. Res., 3(2), 175–180, doi:10.1007/s40003-014-0107-9,

752 2014a.

753 Sharma, S. K., Kumar, M., Rohtash, Gupta, N. C., Saraswati, Saxena, M. and Mandal, T. K.: Characteristics of

754 ambient ammonia over Delhi, India., 2014b.

755 Sharma, S. K., Kotnala, G. and Mandal, T. K.: Spatial Variability and Sources of Atmospheric Ammonia in India:

756 A Review, Aerosol Sci. Eng., 4(1), doi:10.1007/s41810-019-00052-3, 2020.

757 Sherlock, R. R., Freney, J. R., Bacon, P. E. and van der Weerden, T. J.: Estimating ammonia volatilization from

758 unsaturated urea fertilized and urine affected soils by an indirect method, Fertil. Res., 40(3), 197–205,

759 doi:10.1007/BF00750466, 1994.

760 Singh, G. K., Rajeev, P., Paul, D. and Gupta, T.: Chemical characterization and stable nitrogen isotope

761 composition of nitrogenous component of ambient aerosols from Kanpur in the Indo-Gangetic Plains., Sci. Total

762 Environ., 763, 143032, doi:10.1016/j.scitotenv.2020.143032, 2021.

763 Stieger, B., Spindler, G., van Pinxteren, D., Grüner, A., Wallasch, M. and Herrmann, H.: Development of an

764 online-coupled MARGA upgrade for the 2\,h interval quantification of low-molecular-weight organic acids in the

765 gas and particle phases, Atmos. Meas. Tech., 12(1), 281–298, doi:10.5194/amt-12-281-2019, 2019.

766 Sutton, M. A. and Howard, C. M.: Ammonia maps make history, Nature, 564(7734), 49–50, 2018.

767 Sutton, M. A., Burkhardt, J. K., Guerin, D., Nemitz, E. and Fowler, D.: Development of resistance models to

768 describe measurements of bi-directional ammonia surface-atmosphere exchange, Atmos. Environ., 32(3), 473–

769 480, doi:10.1016/S1352-2310(97)00164-7, 1998.

770 Sutton, M. A., Erisman, J. W., Dentener, F. and Möller, D.: Ammonia in the environment: From ancient times to

771 the present, Environ. Pollut., 156(3), 583–604, doi:10.1016/j.envpol.2008.03.013, 2008.

772 Sutton, M. A., Reis, S. and Baker, S. M. H.: Atmospheric Ammonia: Detecting emission changes and

773 environmental impacts., 2009a.

774 Sutton, M. A., Nemitz, E., Milford, C., Campbell, C., Erisman, J. W., Hensen, A., Cellier, P., David, M., Loubet,

775 B., Personne, E., Schjoerring, J. K., Mattsson, M., Dorsey, J. R., Gallagher, M. W., Horvath, L., Weidinger, T.,

776 Meszaros, R., Dämmgen, U., Neftel, A., Herrmann, B., Lehman, B. E., Flechard, C. and Burkhardt, J.: Dynamics

777 of ammonia exchange with cut grassland: synthesis of results and conclusions of the GRAMINAE Integrated

778 Experiment, Biogeosciences, 6(12), 2907–2934, doi:10.5194/bg-6-2907-2009, 2009b.

779 Sutton, M. A., Reis, S., Riddick, S. N., Dragosits, U., Nemitz, E., Theobald, M. R., Tang, Y. S., Braban, C. F.,

780 Vieno, M., Dore, A. J., Mitchell, R. F., Wanless, S., Daunt, F., Fowler, D., Blackall, T. D., Milford, C., Flechard,

781 C. R., Loubet, B., Massad, R., Cellier, P., Personne, E., Coheur, P. F., Clarisse, L., Van Damme, M., Ngadi, Y.,

782 Clerbaux, C., Skjøth, C. A., Geels, C., Hertel, O., Kruit, R. J. W., Pinder, R. W., Bash, J. O., Walker, J. T.,

783 Simpson, D., Horváth, L., Misselbrook, T. H., Bleeker, A., Dentener, F. and de Vries, W.: Towards a climate-

784 dependent paradigm of ammonia emission and deposition, Philos. Trans. R. Soc. B Biol. Sci., 368(1621),

785 20130166–20130166, doi:10.1098/rstb.2013.0166, 2013.

786 Sutton, M. A., Drewer, J., Moring, A., Adhya, T. K., Ahmed, A., Bhatia, A., Brownlie, W., Dragosits, U., Ghude,

787 S. D., Hillier, J., Hooda, S., Howard, C. M., Jain, N., Kumar, D., Kumar, R. M., Nayak, D. R., Neeraja, C. N.,

788 Prasanna, R., Price, A., Ramakrishnan, B., Reay, D. S., Singh, R., Skiba, U., Smith, J. U., Sohi, S., Subrahmanyan,

789 D., Surekha, K., van Grinsven, H. J. M., Vieno, M., Voleti, S. R., Pathak, H. and Raghuram, N.: 2 - The Indian

790 Nitrogen Challenge in a Global Perspective, in The Indian Nitrogen Assessment, edited by Y. P. Abrol, T. K.

791 Adhya, V. P. Aneja, N. Raghuram, H. Pathak, U. Kulshrestha, C. Sharma, and B. Singh, pp. 9–28, Elsevier.,

792 2017a.

793 Sutton, M. A., J. Drewer, A. Moring, T.K Adhya, A. Ahmed and A. Bhatia: The Indian nitrogen assessment :

794 sources of reactive nitrogen, environmental and climate effects, management options, and policies, in The Indian

795 Nitrogen Assessment, edited by Y. P. Abrol, T. K. Adhya, V. P. Aneja, N. Raghuram, H. Pathak, U. Kulshrestha,

796 C. Sharma, and B. Singh, pp. 9–25, Elsevier., 2017b.

797 Sutton, M. A., Van Dijk, N., Levy, P. E., Jones, M. R., Leith, I. D., Sheppard, L. J., Leeson, S., Sim Tang, Y.,

798 Stephens, A., Braban, C. F., Dragosits, U., Howard, C. M., Vieno, M., Fowler, D., Corbett, P., Naikoo, M. I.,

799 Munzi, S., Ellis, C. J., Chatterjee, S., Steadman, C. E., Móring, A. and Wolseley, P. A.: Alkaline air: changing

800 perspectives on nitrogen and air pollution in an ammonia-rich world: Alkaline Air, Philos. Trans. R. Soc. A Math.

801 Phys. Eng. Sci., 378(2183), doi:10.1098/rsta.2019.0315, 2020.

802 Technical specifications for CAAQM station: TECHNICAL SPECIFICATIONS FOR CONTINUOUS

803 AMBIENT AIR QUALITY MONITORING (CAAQM) STATION (REAL TIME) Central Pollution Control

804 Board East Arjun Nagar , Shahdara., 2019.

805 Thomas, R. M., Trebs, I., Otjes, R., Jongejan, P. A. C., Brink, H. ten, Phillips, G., Kortner, M., Meixner, F. X.

806 and Nemitz, E.: An Automated Analyzer to Measure Surface-Atmosphere Exchange Fluxes of Water Soluble

807 Inorganic Aerosol Compounds and Reactive Trace Gases, Environ. Sci. \& Technol., 43(5), 1412–1418,

808 doi:10.1021/es8019403, 2009.

809 Twigg, M. M., Di Marco, C. F., Leeson, S., van Dijk, N., Jones, M. R., Leith, I. D., Morrison, E., Coyle, M.,

810 Proost, R., Peeters, A. N. M., Lemon, E., Frelink, T., Braban, C. F., Nemitz, E. and Cape, J. N.: Water soluble

811 aerosols and gases at a UK background site – Part 1: Controls of PM$_{2.5}$ and PM$_{10}$ aerosol

812 composition, Atmos. Chem. Phys., 15(14), 8131–8145, doi:10.5194/acp-15-8131-2015, 2015.

813 Wagh, S., Singh, P., Ghude, S. D., Safai, P., Prabhakaran, T. and Kumar, P. P.: Study of ice nucleating particles

814   in fog-haze weather at New Delhi, India: A case of polluted environment, Atmos. Res., 259, 105693,

815   doi:https://doi.org/10.1016/j.atmosres.2021.105693, 2021.

816   Wang, Q., Miao, Y. and Wang, L.: Regional transport increases ammonia concentration in Beijing, China,

817   Atmosphere (Basel)., 11(6), doi:10.3390/ATMOS11060563, 2020a.

818   Wang, S., Nan, J., Shi, C., Fu, Q., Gao, S., Wang, D., Cui, H., Saiz-Lopez, A. and Zhou, B.: Atmospheric ammonia

819   and its impacts on regional air quality over the megacity of Shanghai, China, Sci. Rep., 5(October), 1–13,

820   doi:10.1038/srep15842, 2015.

821   Wang, T., Song, Y., Xu, Z., Liu, M., Xu, T., Liao, W., Yin, L., Cai, X., Kang, L., Zhang, H. and Zhu, T.: Why is

822   the Indo-Gangetic Plain the region with the largest NH3column in the globe during pre-monsoon and monsoon

823   seasons?, Atmos. Chem. Phys., 20(14), 8727–8736, doi:10.5194/acp-20-8727-2020, 2020b.

824   Warner, J. X., Dickerson, R. R., Wei, Z., Strow, L. L., Wang, Y. and Liang, Q.: Increased atmospheric ammonia

825   over the world's major agricultural areas detected from space, Geophys. Res. Lett., 44(6), 2875–2884,

826   doi:10.1002/2016GL072305, 2017.

827   Wentworth, G. R., Murphy, J. G., Gregoire, P. K., Cheyne, C. A. L., Tevlin, A. G. and Hems, R.: Soil-atmosphere

828   exchange of ammonia in a non-fertilized grassland: Measured emission potentials and inferred fluxes,

829   Biogeosciences, 11(20), 5675–5686, doi:10.5194/bg-11-5675-2014, 2014.

830   Wentworth, G. R., Murphy, J. G., Benedict, K. B., Bangs, E. J. and Collett, J. L.: The role of dew as a night-time

831   reservoir and morning source for atmospheric ammonia, Atmos. Chem. Phys., 16(11), 7435–7449,

832   doi:10.5194/acp-16-7435-2016, 2016.

833   Xu, J., Chen, J., Huo, J., Lin, Y., Fu, Q., Guo, H. and Lee, S. H.: Importance of gas-particle partitioning of

834   ammonia in haze formation in the rural agricultural environment, Atmos. Chem. Phys., 20(12), 7259–7269,

835   doi:10.5194/acp-20-7259-2020, 2020.

836   Yang, J., Kang, S. and Ji, Z.: Sensitivity analysis of chemical mechanisms in the WRF-chem model in

837   reconstructing aerosol concentrations and optical properties in the Tibetan Plateau, Aerosol Air Qual. Res., 18(2),

838   505–521, doi:10.4209/aaqr.2017.05.0156, 2018.

839   Zhang, X., Liu, J., Han, H., Zhang, Y., Jiang, Z., Wang, H., Meng, L., Li, Y. C. and Liu, Y.: Satellite-Observed

840   Variations and Trends in Carbon Monoxide over Asia and Their Sensitivities to Biomass Burning, Remote Sens.,

841   12(5), 830, doi:10.3390/rs12050830, 2020.

842

843

844

845

846

847

848

849

850

FIGURE CAPTIONS

Figure 1. (a) Comparison of observed and simulated average diurnal variation in (a) meteorological parameters such as Temperature (T in °c) and Relative humidity (RH in %) and (b) NH_3 and NH_4^+ concentration (µg m^{-3}) during the sampling period (bar indicates mean standard deviation of each hour).

Figure 2. Ratio of model/obs of the daily mean NH_3, NH_4^+ and total NH_x concentration

Figure 3. Share of major components of gases and particulate matter (PM$_{2.5}$) based on the mean concentrations during WiFEX (share according to µeq m^{-3}).

Figure 4. Fraction HCl/Cl$^-$ ratio as a function of NH_4^+ concentration (µg m^{-3}) and Relative humidity (RH)

Figure 5. Bivariate plots of mean (a) NH_3 concentration (b) NH_4^+ concentration (c) Cl$^-$ concentration and (d) total NH_x concentration in relation to wind speed (m s^{-1}) and direction.

Figure 6. Neutralizing effect between Cl$^-$, NO_3^- and SO_4^{2-} as the anions (µɛq m^{-3}) and aerosol neutralization ratio (ANR) where, ANR>1 indicates over neutralized (alkaline) and ANR<1 indicates under neutralized (acid) (orange bar indicates daily mean standard error).

Figure 7. Box-Whiskers plot for trace gases and secondary inorganic aerosols from the observations (MARGA) and simulated in sensitivity test with changes in HCl emissions (No HCl (0 mol km^{-2} h^{-1}), Base Case HCl (24.8 mol km^{-2} h^{-1}), and 3×Base HCl (74 mol km^{-2} h^{-1})) at IGIA, Delhi.

Figure 8. (top) Average diurnal cycles of NH_3 and NH_4^+ concentration (µg m^{-3}) with mole equivalents of Cl$^-$, NO_3^-, SO_4^{2-}, NH_4^+, SO_2, HCl and HNO_3 (µeq m^{-3}) of (a) measured (MARGA) and (b) modeled (3×Base HCl run) along with its meteorological parameters (bottom).

Figure 9. Diurnal variation in the mean (a) NH_3 concentration (b) NH_4^+ concentration and (c) total NH_x concentration observed (black), simulated in No HCl (red dotted), Base Case HCl (red dash) and 3×Base HCl run (red solid).

Figure 10. Comparison of ratio of model/obs in the daily mean (a) NH_3 concentration (b) NH_4^+ concentration and (c) total NH_x concentration in 3×Base HCl and -3×NH$_3$_EMI scenario.

 TABLES

 Table 1. Performance statistics of correlation coefficient (*r*) of NH$_4^+$/NH$_x$ with NH$_3$ and aerosols (NH$_4^+$, Cl$^-$

 , SO$_4^{2-}$, and NO$_3^-$)

894

Gases and Aerosols	MARGA Correlation coefficient (*r*) with NH$_4^+$/NH$_x$ ratio	Model Correlation coefficient (*r*) with NH$_4^+$/NH$_x$ ratio
Ammonia (NH$_3$)	-0.57	-0.58
Ammonium (NH$_4^+$)	0.70	0.67
Chloride (Cl$^-$)	0.79	-
Sulfate (SO$_4^-$)	0.09	0.77
Nitrate (NO$_3^-$)	0.13	0.57

895
896
897
898
899
900
901
902
903
904
905
906
907
908
909
910
911
912
913
914
915
916
917
918
919

920 **Table 2. Daily mean $\pm 1\sigma$ in gases and inorganic aerosol concentration observed (MARGA) and simulated**
921 **in sensitivity test with changes in total HCl emissions (No HCl (0 mol km^{-2} h^{-1}), Base Case HCl (24.8 mol**
922 **km^{-2} h^{-1}), and 3×Base HCl (74 mol km^{-2} h^{-1}).**

923

Species concentration (μg m^{-3})	MARGA	No HCl	Base Case HCl	3×Base HCl
NH_3	20 ± 8.52	50.2 ± 11.7	48.2 ± 11.31	44.5 ± 10.8
NH_4^+	35.9 ± 17.7	13.9 ± 3.04	21.4 ± 6.65	34.5 ± 15.2
NH_x	56.6 ± 17.1	64 ± 13.2	69.6 ± 16.6	79.5 ± 23.7
Cl^-	50.6 ± 39.4	-	15.1 ± 9.65	40.9 ± 27.2
NO_3^-	27.9 ± 8.17	35.9 ± 7.23	35.6 ± 7.05	35.5 ± 7.03
SO_4^{2-}	17.1 ± 5.63	9.62 ± 2.78	9.56 ± 2.71	9.56 ± 2.71
HCl	0.86 ± 0.35	-	0.20 ± 0.23	0.22 ± 0.25
HNO_3	3.43 ± 1.68	0.18 ± 0.21	0.17 ± 0.22	0.18 ± 0.23
SO_2	30.6 ± 18.4	46.6 ± 12.4	46.7 ± 12.4	46.7 ± 12.4

924
925
926
927
928
929
930
931
932
933
934
935
936
937
938
939
940
941

942 **Table 3. Model performance statistics for NH_3, NH_4^+ and total NH_x concentration at IGIA, Delhi from three**

943 **sensitivity experiments (No HCl (0 mol km^{-2} h^{-1}), Base Case HCl (24.8 mol km^{-2} h^{-1}), and 3×Base HCl (74**

944 **mol km^{-2} h^{-1})) and the MARGA**

945

Species	No HCl		Base Case HCl		3×Base HCl	
	Correlation coefficient (*r*)	Normalised Mean Bias (NMB)	Correlation coefficient (*r*)	Normalised Mean Bias (NMB)	Correlation coefficient (*r*)	Normalised Mean Bias (NMB)
NH_3	-0.58	1.38	-0.60	1.29	-0.65	1.13
NH_4^+	0.45	-0.61	0.75	-0.40	0.76	-0.03
NH_x	0.69	0.12	0.70	0.22	0.70	0.39

946
947
948
949
950
951
952
953
954
955
956
957
958

959   **Figure 1**
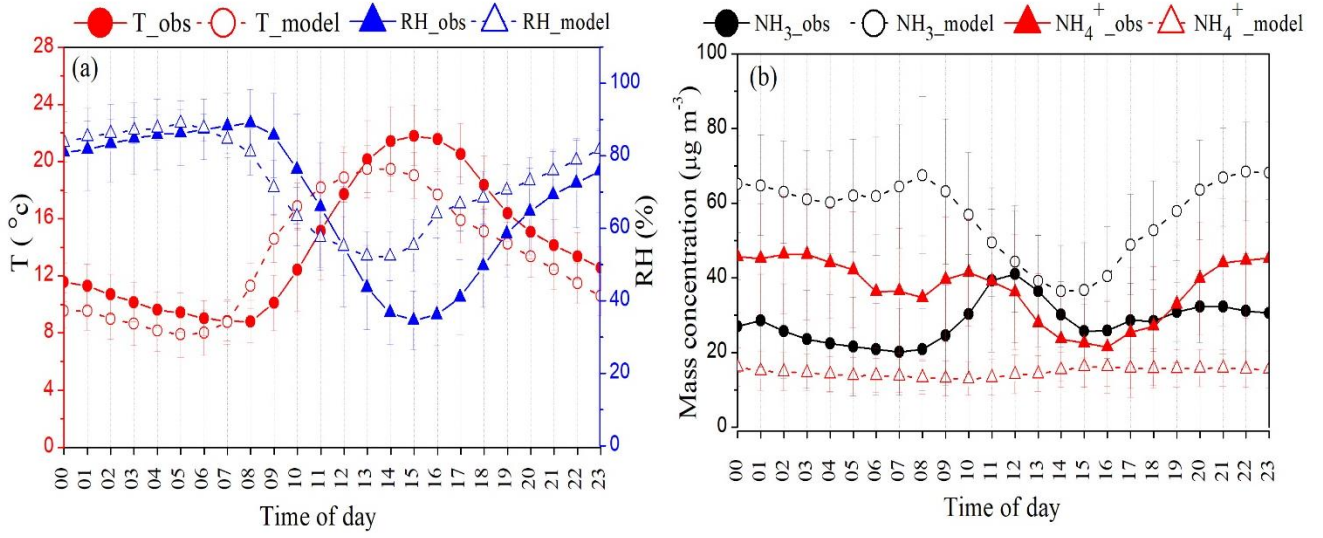
960
961

962   **Figure 2**
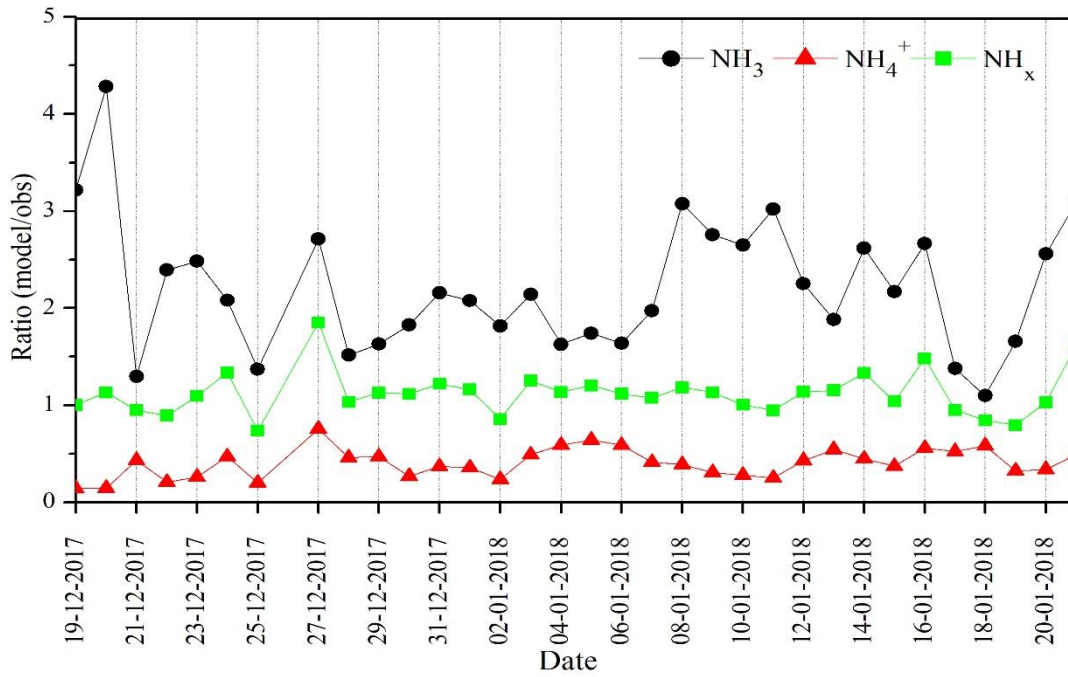
963
964
965
966

967 **Figure 3**
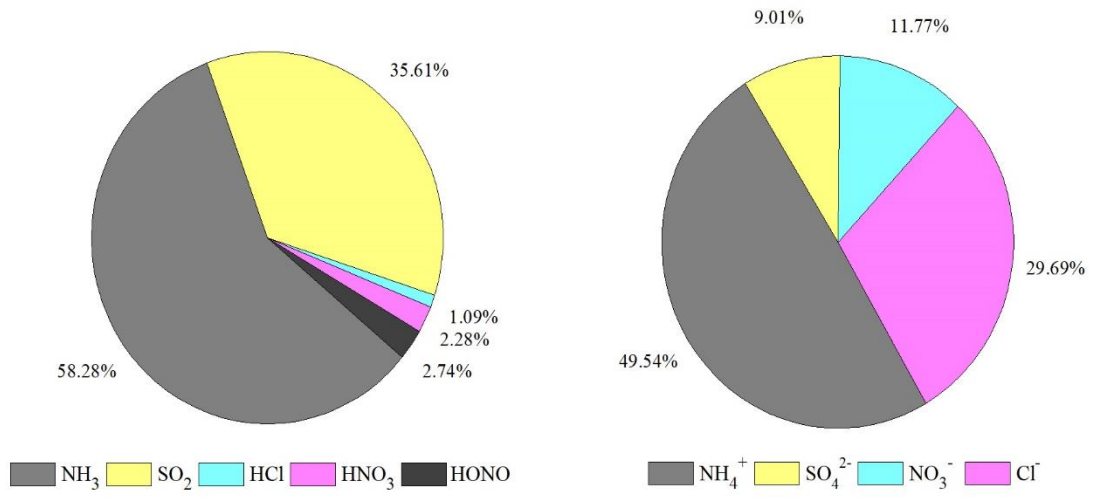
968
969
970

971 **Figure 4**
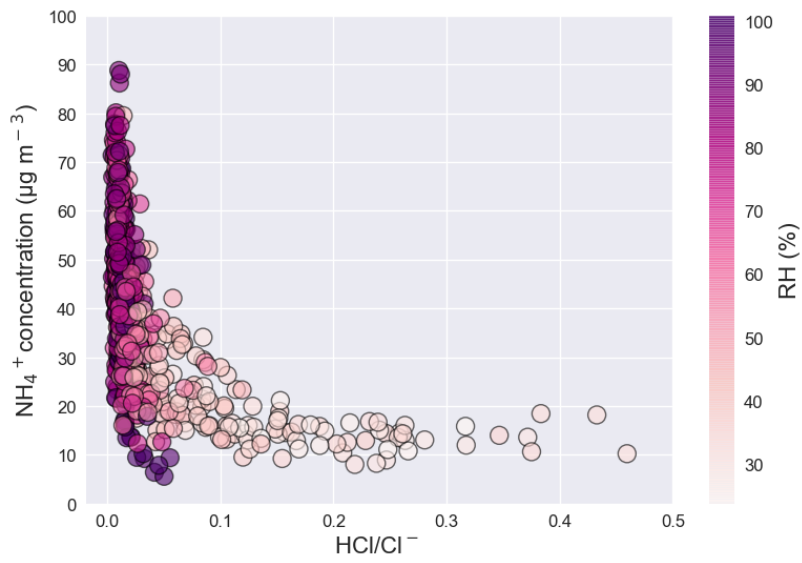
972
973

974

975

976 **Figure 5**
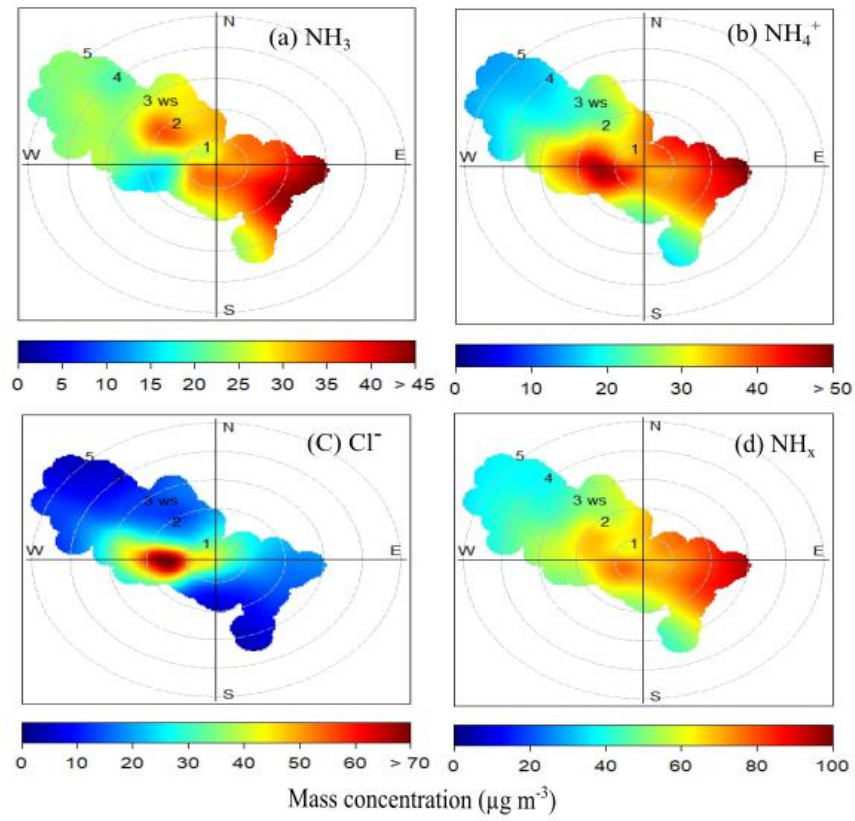
977

978 **Figure 6**

979
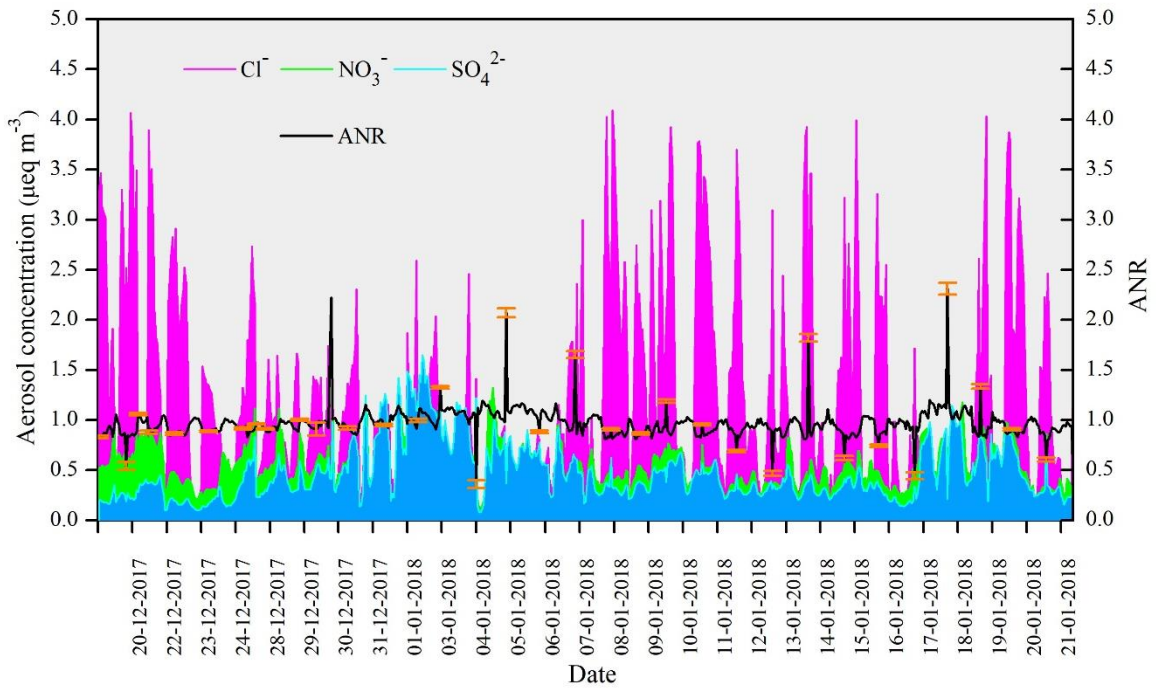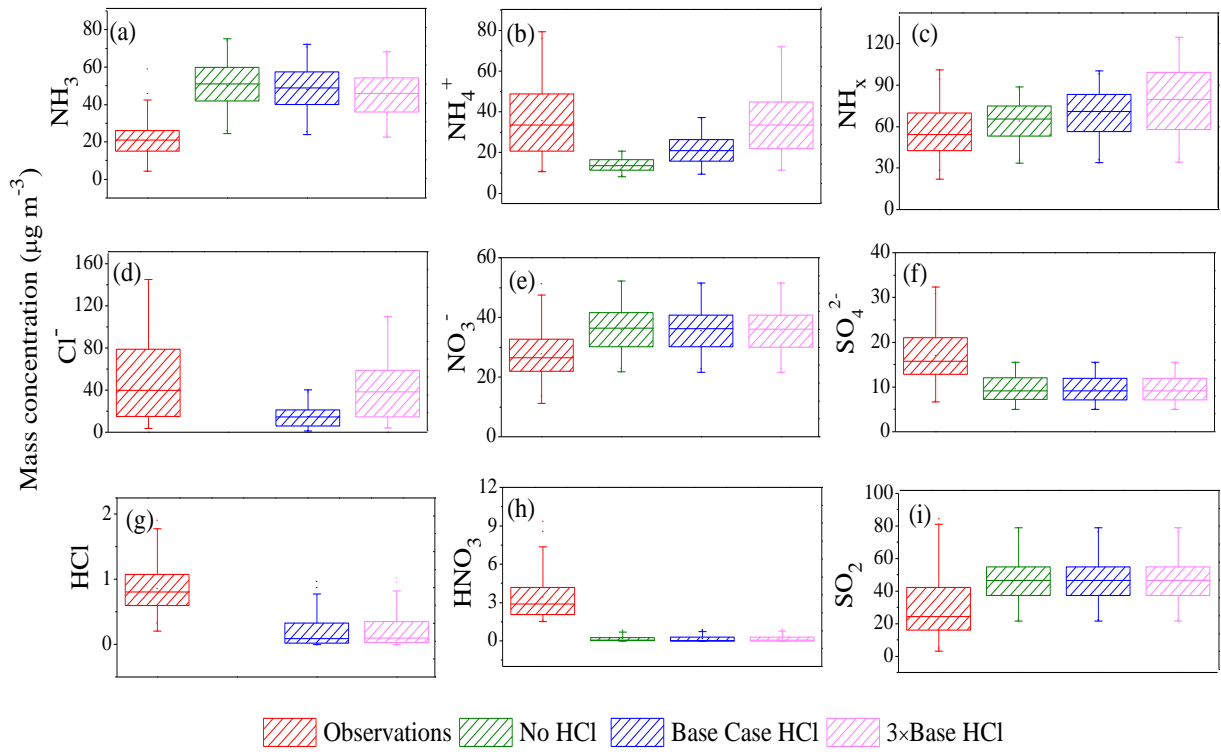
 Figure 7

981
982   v
983
984
985
986
987
988
989
990
991
992
993
994
995
996
997
998
999
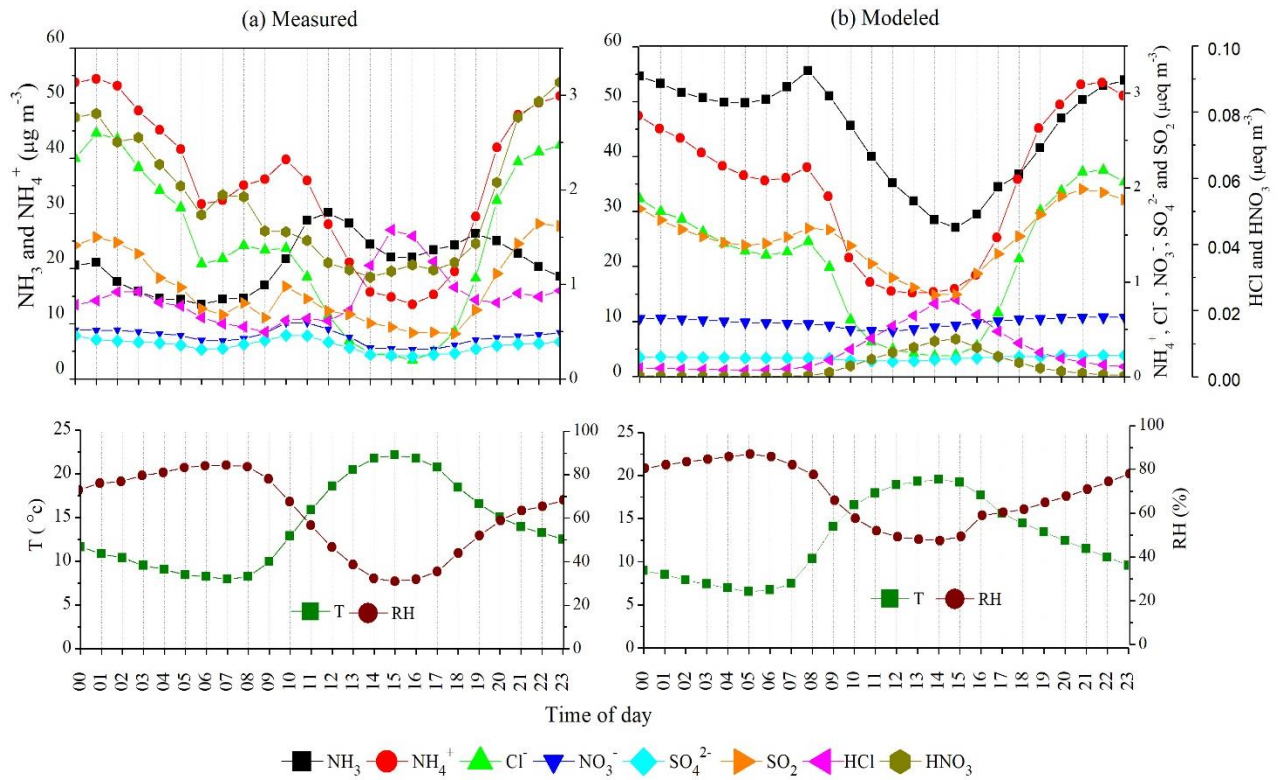
1000   **Figure 8**

1020   **Figure 9**
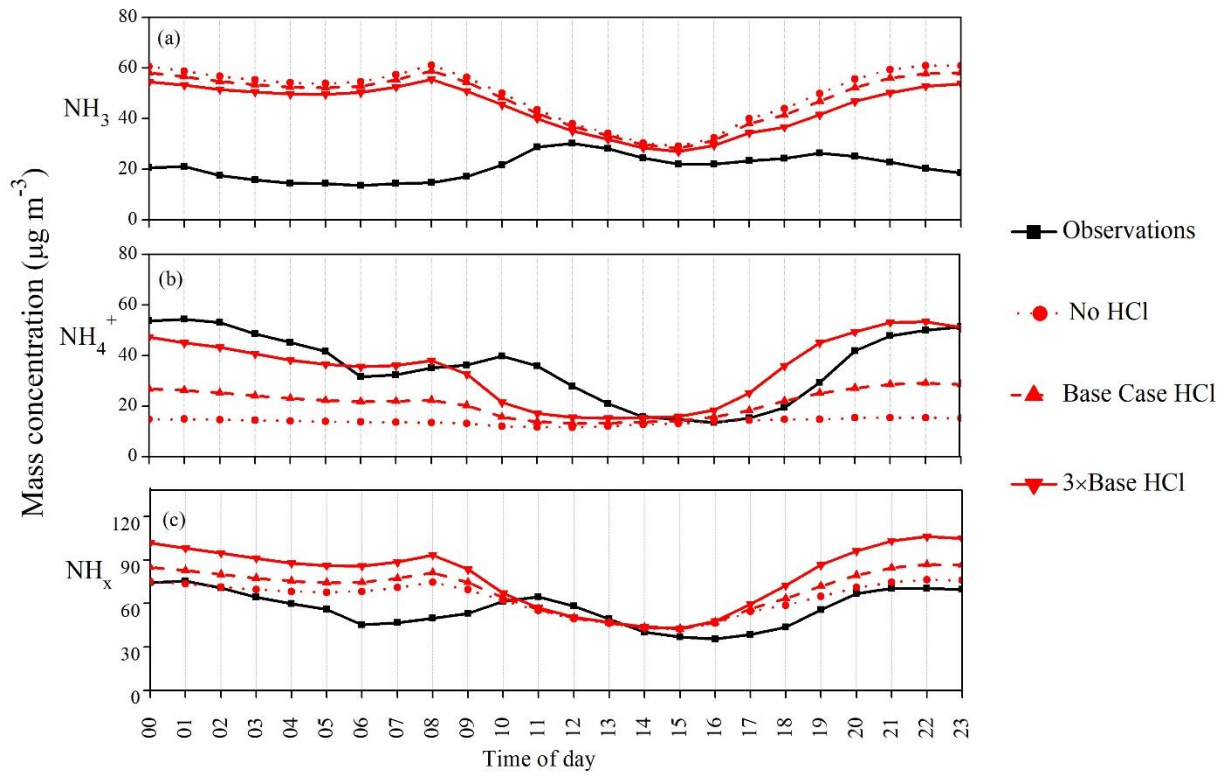
1021

1022

1023

1024

1025

1026

1027

1028

1029

1030

1031

1032

1033

1034

1035

1036

1037 **Figure 10**
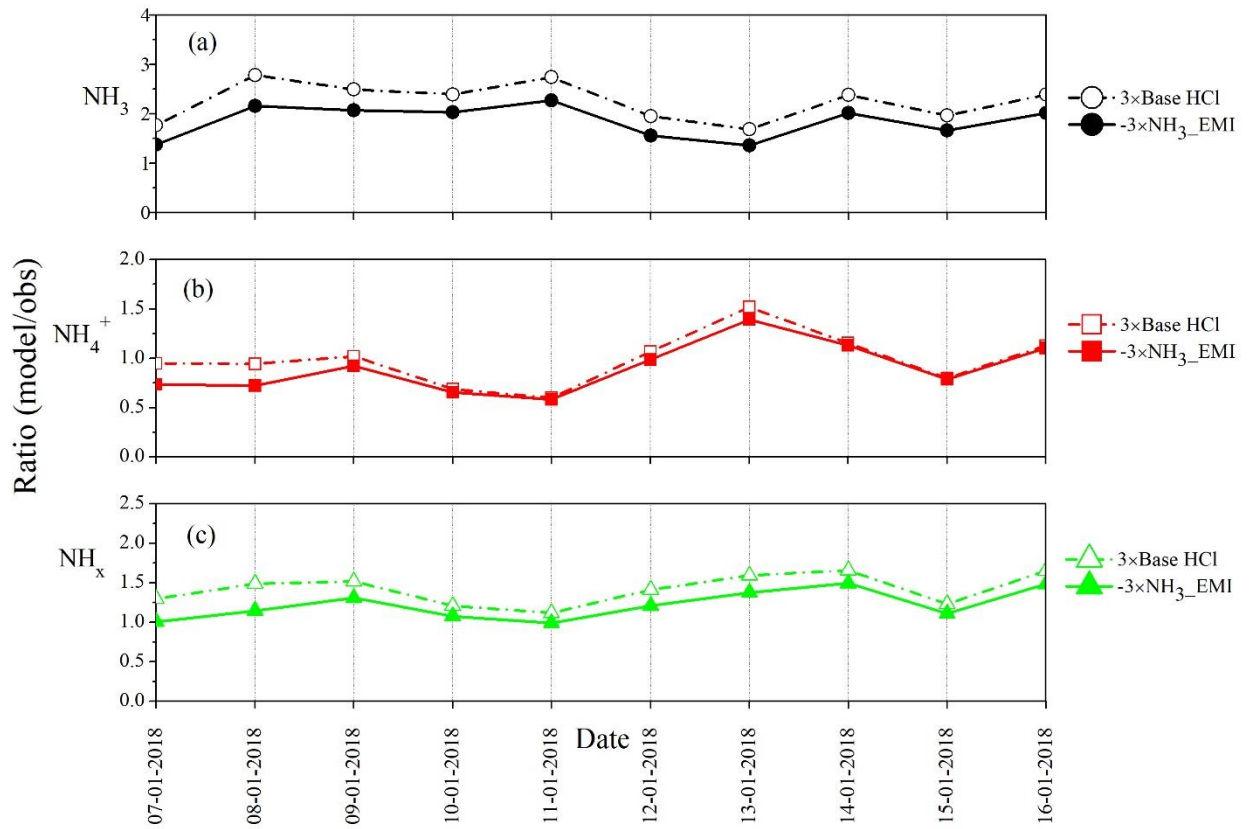
1038
1039
1040
1041
1042
1043
1044
1045
1046